ACS NANOSCIENCE Au
AN OPEN ACCESS JOURNAL OF THE AMERICAN CHEMICAL SOCIETY

pubs.acs.org/nanoau Article

Robust Nanoparticle-Derived Lubricious Antibiofilm Coating for Difficult-to-Coat Medical Devices with Intricate Geometry

Hossein Yazdani-Ahmadabadi, Kai Yu, Sara Khoddami, Demian F. Felix, Han H. Yeh, Haiming D. Luo, Igor Moskalev, Qiong Wang, Rizhi Wang, Dana Grecov, Ladan Fazli, Dirk Lange,* and Jayachandran N. Kizhakkedathu*

Cite This: *ACS Nanosci. Au* 2023, 3, 67–83 Read Online

ACCESS | Metrics & More | Article Recommendations | Supporting Information

ABSTRACT: A major medical device-associated complication is the biofilm-related infection post-implantation. One promising approach to prevent this is to coat already commercialized medical devices with effective antibiofilm materials. However, developing a robust high-performance antibiofilm coating on devices with a nonflat geometry remains unmet. Here, we report the development of a facile scalable nanoparticle-based antibiofilm silver composite coating with long-term activity applicable to virtually any objects including difficult-to-coat commercially available medical devices utilizing a catecholic organic–aqueous mixture. Using a screening approach, we have identified a combination of the organic–aqueous buffer mixture which alters polycatecholamine synthesis, nanoparticle formation, and stabilization, resulting in controlled deposition of in situ formed composite silver nanoparticles in the presence of an ultra-high-molecular-weight hydrophilic polymer on diverse objects irrespective of its geometry and chemistry. Methanol-mediated synthesis of polymer–silver composite nanoparticles resulted in a biocompatible lubricious coating with high mechanical durability, long-term silver release (~90 days), complete inhibition of bacterial adhesion, and excellent killing activity against a diverse range of bacteria over the long term. Coated catheters retained their excellent activity even after exposure to harsh mechanical challenges (rubbing, twisting, and stretching) and storage conditions (>3 months stirring in water). We confirmed its excellent bacteria-killing efficacy (>99.999%) against difficult-to-kill bacteria (*Proteus mirabilis*) and high biocompatibility using percutaneous catheter infection mice and subcutaneous implant rat models, respectively, *in vivo*. The developed coating approach opens a new avenue to transform clinically used medical devices (e.g., urinary catheters) to highly infection-resistant devices to prevent and treat implant/device-associated infections.

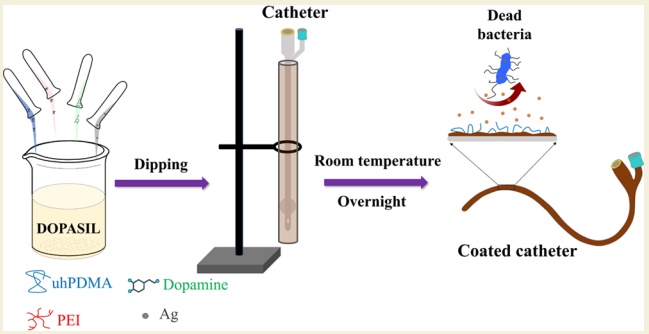

KEYWORDS: *implant/device-associated infection, antibiofilm coating, nanoparticle stabilization, sustained silver release, durable substrate-independent silver coating, long-term prevention of infection, water-miscible organic solvent*

INTRODUCTION

One major concern for the clinical use of medical devices (e.g., indwelling catheters) is the high risk of post-implantation infection.[1−4] Despite superior mechanical properties of the clinically approved indwelling catheters, they are shown to be ineffective in the prevention of biofilm formation over the long term (>7 days).[5,6] With this, one promising approach to address this concern without intervention in the catheter manufacturing process is to exclusively modify the surface of already commercialized catheters with highly effective antibiofilm coatings. However, coating such devices remains a challenge due to their hydrophobic surface, absence of reactive functional groups, and intricate geometries. The important catheter antibiofilm coatings attempted so far include antimicrobial peptides,[7−9] polycations,[10−12] hydrogels,[13] hydrophilic polymer assemblies/brush-like structures,[14−18] metallic nanoparticles,[19−21] ultra-low surface energy materials,[22−24] nitric oxide-releasing coatings,[25] and light-triggered photothermal coatings.[26−28] Smith *et al.* developed a highly hydrophilic brush-like polymeric coating for polyurethane (PU) vascular catheters utilizing a multi-step specific coating process.[15] Despite the improved short-lived efficacy (1−3 log reduction in bacterial adhesion within 24 h), the coating was not applicable to nonpolymeric materials as the substrate requires significant solvent [e.g., isopropanol (IPOH)] diffusivity to initiate surface polymerization. Geyer

Received: August 16, 2022
Revised: October 12, 2022
Accepted: October 13, 2022
Published: October 28, 2022

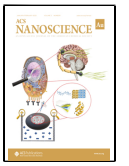

https://doi.org/10.1021/acsnanoscienceau.2c00040
ACS Nanosci. Au 2023, 3, 67–83

et al. reported the generation of a superhydrophobic silica coating on PU catheters.[22] They showed that the coating effectively inhibited *Escherichia coli* adhesion for a week. However, this coating process was highly water-sensitive in the parts per million level and was not universal as the coating composition was highly dependent on the surface chemistry of the substrate. Despite the outstanding activity of the coating in the short term (<7 days), there is a high risk of bacterial adaptation with time (>7 days) as the coating lacks antimicrobial agents. Yong *et al.* utilized photo-curable systems to generate a tough hydrogel applicable to silicone catheters.[13] The surface of the hydrogel-coated catheter showed great antibacterial activity in the early stage (24 h), followed by a significant decrease after 3 days. Tan *et al.* developed a noninvasive photothermal red phosphorous coating solution applicable to metallic implants (e.g., titanium) to eradicate the already formed biofilm by exposing to near-infrared light (laser wavelength: 808 nm) as the biofilm prevention failed. Despite therapeutic capability of this coating, its application to nonflat polymeric devices (e.g., silicone catheters) is poor. Given the poor scalability and adaptability of the attempted coatings to diverse substrates along with short-term antibiofilm activity (<7 days), the need for the development of a scalable facile antibiofilm coating with long-term activity and high adaptability to medical devices with intricate geometry remains unmet.

We previously utilized catechol chemistry in combination with ultra-high-molecular-weight hydrophilic polymers to generate a universal antibiofilm coating.[29] We further attempted to improve the antibacterial efficacy and extend the length of action of this binary coating by incorporating silver which is known to be a strong bactericide.[30−32] We demonstrated the facile generation of a coating called SAFE coating that offers a sustained silver release profile. The combination of sustained silver release and surface enrichment with antifouling polymers fully inhibited bacterial growth on the surface over the long term. The SAFE components included dopamine (DA), silver nitrate, low-molecular-weight polyethylenimine (LMW-PEI), and ultra-high-molecular-weight poly(*N*,*N*-dimethylacrylamide) (PDMA) (uhPDMA). DA was utilized as a binder and an adhesion promoter since catechol-containing molecules such as DA are well known for their strong adhesion to diverse materials, good biocompatibility, and self-polymerization.[33] Given this, DA chemistry has been utilized for the development of antibacterial coatings with great versatility and increased stability.[34,35] LMW-PEI was used as the crosslinking agent because of its high chemical reactivity toward polydopamines,[36] while silver was incorporated due to its strong antibacterial activity against diverse bacterial species. Silver nanoparticles/clusters were synthesized from silver nitrate in situ during the early stage of DA oxidation and polymerization. The incorporation of uhPDMA into the SAFE coating was aimed to endow the SAFE coating with antifouling function. Our previous mechanistic studies showed that all four SAFE components were essential for achieving the high antibiofilm activity.[29] Despite excellent long-term antibiofilm activity, scalability, and adaptability of the SAFE coating to flat materials, coating nonflat surfaces with the SAFE composition requires a multi-step coating procedure. For instance, to coat a full-size catheter with the SAFE composition, the coating process should be repeated at least four times for achieving the full coverage of the surface. The catheter should be turned around 90° after each coating process so that the other side is coated. We observed that the SAFE coating process resulted in uncontrolled deposition of already formed SAFE assemblies to form a porous coating with ineffective coverage on difficult-to-coat nonflat surfaces in a one-step dipping process.

To address this, the present work describes the development of a new generation of antibiofilm coatings based on the SAFE coating composition with excellent durability that can be applied to virtually any object and nonflat articles with intricate geometries including medical devices *via* a one-step coating process. Our hypothesis was that the modification of the oxidation/polymerization of DA, subsequent self-assembly, and stabilization of PDA nanoparticles and film formation would result in a robust coating. One strategy to modulate this is to change the synthesis parameters such as pH, temperature, and coating time.[37,38] Another approach is to leverage the combination of DA with off-the-shelf chemicals such as oxidants, hydrophilic polymers, nanoparticles, and so forth.[39,40] Despite great advances achieved using these strategies, the incorporation of such chemicals might impair the unique properties of PDA (universality, versatility, and strong adherence). Here, we describe a new nanoparticle-based coating process in the water-soluble organic−aqueous mixture to generate an antibiofilm coating with high stability, lubricity, and long-term activity, which can be applied to virtually all objects irrespective of its geometry and chemistry.

RESULTS

Design and Development of Durable One-Pot Antibiofilm Solvent-Induced Long-Acting Coating

Our objective was to modulate PDA synthesis and the nanoparticle assembly formation while maintaining its intrinsic properties such as excellent adhesion to the diverse underlying materials. We aimed to combine a water-soluble organic solvent with SAFE components[35,36] for achieving the controlled PDA synthesis and a coating with high stability and activity. We screened diverse water-miscible organic solvents in combination with Tris buffer to change the solution properties such as surface tension, oxygen solubility, DA solubility, and hydroxide content, which significantly affects the PDA synthesis, particle formation, and deposition. Decreasing the surface tension of the coating solution is anticipated to enhance surface wetting and coating adherence.[41] Similarly, a reduction in the hydroxide content or oxygen solubility in the solvent mixture could result in the decreased rate of DA oxidation/polymerization.[38] Using this coating method, we showed the ability to develop a robust antibiofilm coating on any surface irrespective of its geometry and chemical nature resulting in excellent protection from the attachment of both Gram-negative and -positive bacterial species. We named the coating durable one-pot antibiofilm solvent-induced long-acting (DOPASIL) coating. Furthermore, we demonstrate the high durability of the DOPASIL coating with excellent long-term activity in various conditions. The high biocompatibility and antibiofilm efficacy of the DOPASIL coating are also confirmed *in vivo*.

Our hypothesis was that the control of formation and deposition of in situ formed nanoparticles during catechol polymerization and crosslinking would result in a stable and durable coating on diverse surfaces. For this, we introduced a water-miscible organic solvent to the SAFE composition [DA (2 mg/mL), LMW-PEI (1.5 mg/mL), silver nitrate (0.5 mg/mL), and uhPDMA (5 mg/mL)] as organic solvents are

https://doi.org/10.1021/acsnanoscienceau.2c00040
ACS Nanosci. Au 2023, 3, 67−83

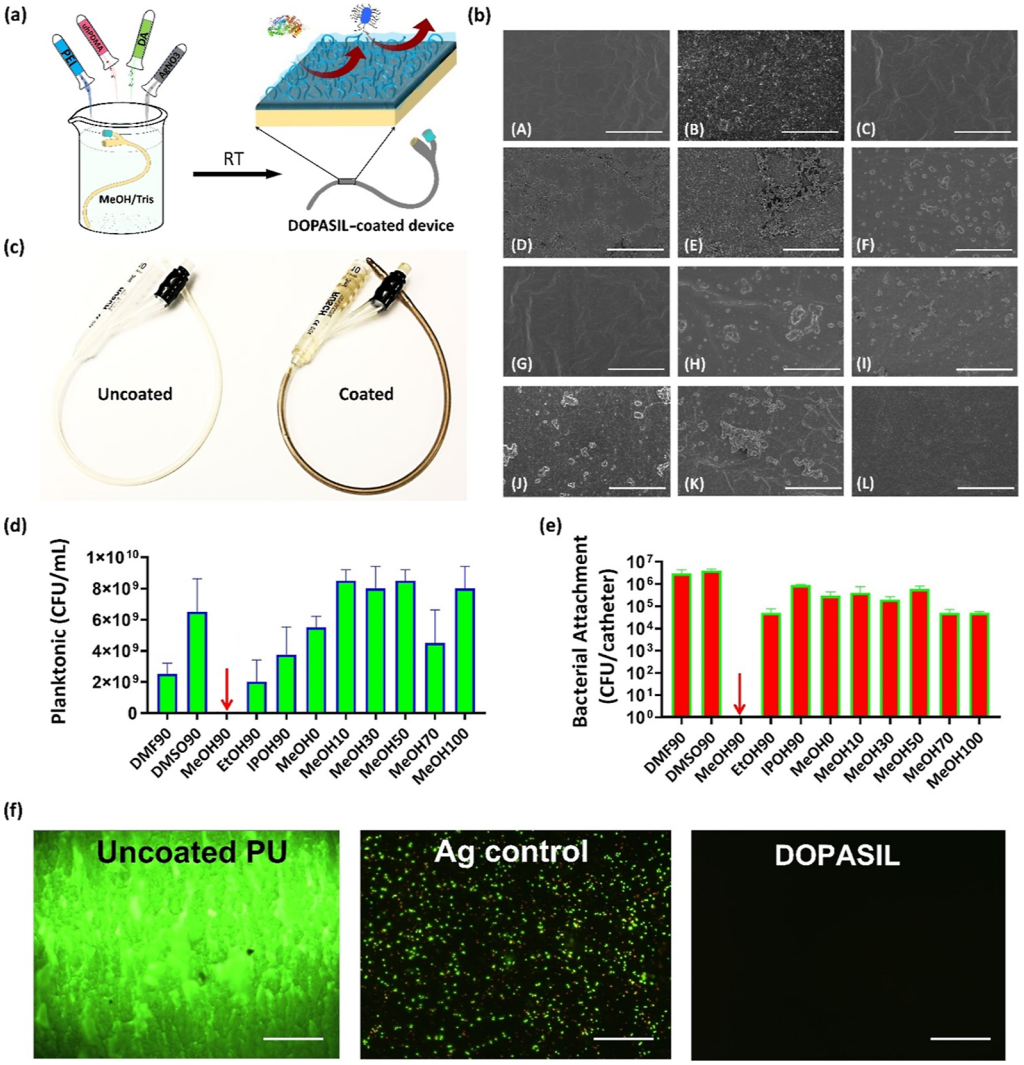

Figure 1. Development of the DOPASIL coating. (a) Schematic representation for the preparation of the DOPASIL coating: four components including DA, LMW-PEI, silver nitrate, and uhPDMA were mixed. The substrate (e.g., a silicone urinary catheter) was immersed in a coating solution for 24 h at room temperature to generate the highly hydrophilic anti-adhesive DOPASIL coating with long-term activity (b) SEM images of (A) uncoated and coated silicone urinary catheters treated with compositions containing different water-miscible organic solvents at different solvent/Tris ratios. The coating composition contained DA (2 mg/mL), PEI (1.5 mg/mL), silver nitrate (0.5 mg/mL), uhPDMA (5 mg/mL), and solvent/Tris solution: (B) DMF90/Tris10, (C) DMSO90/Tris10, (D) methanol90/Tris10, (E) ethanol90/Tris10, (F) isopropanol90/Tris10, (G) Tris alone, (H) methanol10/Tris90, (I) methanol30/Tris70, (J) methanol50/Tris50, (K) methanol70/Tris30, and (L) MeOH alone. The scale bar is 10 μm. (c) Digital images of a full-size 10 Fr silicon urinary catheter before (left image) and after (right image) coating with the DOPASIL solution. (d) Concentration of planktonic bacteria present in the culture media wherein the silicone urinary catheter is coated with different coatings incubated with *E. coli* (1×10^6 CFU/mL, LB, 500 μL) for 7 days. (e) Number of bacterial colonies adhered to the surface of the coated silicone urinary catheter with different coating compositions incubated with *E. coli* for 7 days (initial concentration: 1×10^6 CFU/mL, LB, 500 μL). The red arrow indicates null planktonic-surface-attached bacteria. (f) Fluorescence images of biofilm formation on the surface of uncoated, Ag control-coated, and DOPASIL (MeOH90/Tris10)-coated PU sheets after 7 days of incubation with *E. coli* (initial concentration: 1×10^6 CFU/mL, LB, 500 μL). The scale bar is 100 μm.

known to slow the oxidation of catechol and subsequent nanoparticle formation.[42−44] Given the fact that the high rate of DA oxidation in aqueous basic conditions is mainly due to the presence of hydroxide ions acting as a catalyst for DA polymerization, a decrease in the hydroxide ion concentration could reduce the rate of DA oxidation/polymerization and is anticipated to control the assembly of in situ formed nanoparticles. The replacement of a part of the basic buffer solution with a water-miscible organic solvent was utilized to limit the number of hydroxide ions present in the coating solution and to regulate the intramolecular interactions of PDA.

We initially screened several organic solvents to identify the optimal water-miscible solvent that works well in combination with the SAFE composition in aqueous solution to generate the DOPASIL coating. To prepare the DOPASIL coating, the substrate of interest (e.g., a silicone urinary catheter) was placed overnight at room temperature in a solution containing DA (2 mg/mL), LMW-PEI (1.5 mg/mL), silver nitrate (0.5 mg/mL), uhPDMA (5 mg/mL), and the solvent system (Figure 1a). We tested several commonly used water-miscible organic solvents [methanol (MeOH), ethanol (EtOH), IPOH, dimethylformamide (DMF), and dimethyl sulfoxide (DMSO)]

https://doi.org/10.1021/acsnanoscienceau.2c00040
ACS Nanosci. Au 2023, 3, 67−83

with a different surface tension, oxygen solubility, and DA solubility (Table 1).

Table 1. Characteristics of the Solvents Used in the Screening Studies[45−47]

solvent	surface tension at 20 °C (mN/m)	oxygen solubility (mole fraction)	DA solubility (mg/mL)
water	72.8	4×10^{-5}	~15
MeOH	22.7	4.2×10^{-4}	~20
EtOH	22.1	5.8×10^{-4}	~2
IPOH	23	7.8×10^{-4}	
DMF	37.1	3.9×10^{-4}	~30
DMSO	43.54	9×10^{-5}	~30

The coating formed in the absence of uhPDMA is called Ag control. We utilized scanning electron microscopy (SEM) to identify the optimal solvent and solvent/Tris buffer ratio in terms of coating features (compactness and uniformity). Among the diverse solvents tested in combination with SAFE, MeOH was found to provide the most uniform coating structure (Figure 1b, image D) compared to other solvents or conditions tested. Unlike the MeOH/Tris 90:10 v/v solution, the SAFE solution did not form a coating with similar thickness following vertical placement in the coating solution (Figure 1b, image G). Overall, the thickness and uniformity of the SAFE coating were strongly dependent on the position of the catheter in solution and how many times the coating process was repeated as described earlier. In comparison, one key advantage of the DOPASIL-coating process is that the placement of the whole catheter in the MeOH/Tris 90:10 v/v solution in any position (vertical, horizontal, or tilted) results in the entire device being coated *via* the one-step-dip-coating process. This comparison obviously showed the important role of the organic solvent in improving coating characteristics on nonflat surfaces. While some microparticles were observed on the surface of the catheter treated with a coating composition containing EtOH, IPOH, and DMF, they failed to form as uniform a layer with great surface coverage as that formed using the MeOH/Tris 90:10 v/v solution (Figure 1b, images B, E, and F). Among the different solvents (90% v/v) tested, the solvent with the lowest surface tension, moderate DA solubility, and highest oxygen solubility (e.g., MeOH) resulted in the best outcome. As shown in Figure 1c, the full-size 10 Fr silicone urinary catheter is fully covered with a brownish material which is indicative of DOPASIL coating. We next investigated the efficacy of the silicone urinary catheters coated with diverse compositions to resist the adhesion of *E. coli* [1×10^6 colony forming unit (CFU)/mL as the starting concentration] over a 7-day period utilizing CFU counts and fluorescence microcopy (Figure 1d). Overall, the DOPASIL coating formed using MeOH/Tris 90:10 v/v showed the best

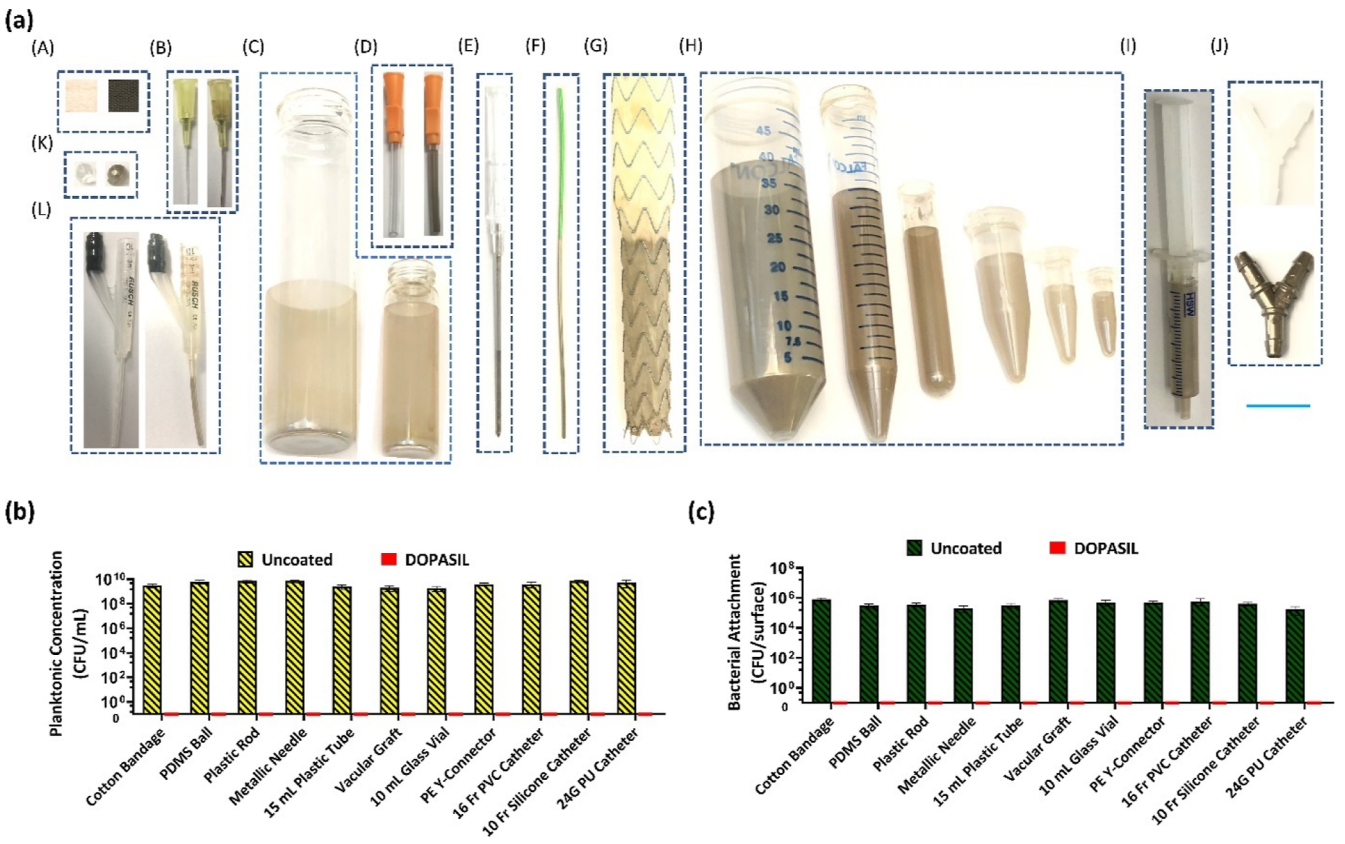

Figure 2. Applicability/versatility of the DOPASIL coating. (a) Digital images of diverse objects coated with the DOPASIL composition: (A) bandage [uncoated (left) and coated (right)], (B) 24G IV PU catheter [uncoated (left) and coated (right)], (C) glass vials with two different sizes, (D) pieces of the 16 Fr PVC urinary catheter [uncoated (left) and coated (right)], (E) metallic needle (the half bottom portion coated), (F) green plastic rod (the half bottom portion coated), (G) vascular graft (the half bottom portion coated), (H) plastic tubes with six different sizes, (I) 6 mL norm-jet syringe, (J) Y-shaped connectors [uncoated (top), (K) PDMS ball (diameter: 5 mm) and coated (bottom)], (L) pieces of the 10 Fr silicone urinary catheter [uncoated (left) and coated (right)]. The blue scale bar is 2 cm. The number of (b) planktonic colonies and (c) surface-attached bacteria for uncoated/DOPASIL-coated objects after 24 h of incubation with *E. coli* (1×10^6 CFU/mL).

https://doi.org/10.1021/acsnanoscienceau.2c00040
ACS Nanosci. Au 2023, 3, 67−83

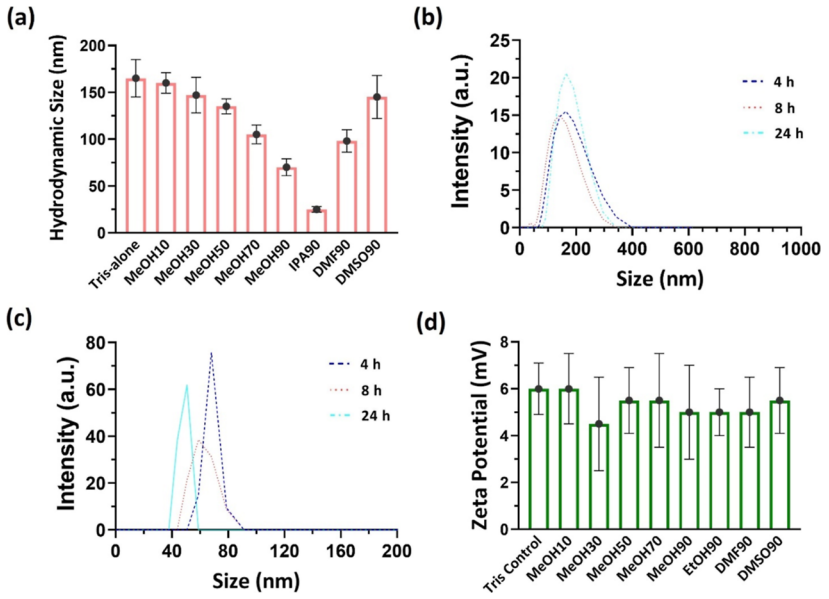

Figure 3. Characteristics of nanoparticles formed in the presence of different organic−buffer mixtures. (a) Hydrodynamic size of DOPASIL nanoparticles formed in solutions containing different solvents and at different solvent/Tris ratios. Size distribution of DOPASIL nanoparticles formed (b) in the absence of the water-miscible organic solvent and (c) in the presence of 90% MeOH at different time points. (d) ζ potential of DOPASIL nanoparticles formed in solutions containing different solvents and at different solvent/Tris ratios.

results, completely suppressing planktonic growth and bacterial adhesion on the surface of the device (Figure 1d,e). The fluorescence microscopy analysis further confirmed the excellent anti-adhesive and antibacterial activity of the DOPASIL coating against *E. coli*, with no bacteria evident on the DOPASIL-coated surface. In contrast, significant bacterial biomass was evident on the uncoated surface and that containing the Ag control coating (without uhPDMA) (Figure 1f).

Adaptability of the DOPASIL Coating

We next verified that the DOPASIL coating can be effectively applied to diverse objects/materials with different chemistries, geometries, and varying sizes. The objects used include a bandage, a 24G intravenous (IV) PU catheter, glass vials with different sizes, a 16 Fr polyvinyl chloride (PVC) urinary catheter, a metallic needle, a plastic rod, a vascular graft, plastic tubes with different sizes, a 6 mL norm-jet syringe, a Y-shaped medical connector, a polydimethylsiloxane (PDMS) ball, a 10 Fr silicone urinary catheter, and 3D-printed objects made of the acrylonitrile−butadiene−styrene terpolymer. The surface of the coated objects was found to be effectively covered with a brownish layer which supports the DOPASIL-coating formation (Figures 2a and S1). We also assessed the antibacterial and anti-adhesion efficacy of the DOPASIL coating on various objects against *E. coli* (1×10^6 CFU/mL, LB, 24 h). For all coated objects, no planktonic bacteria were left in solution 24 h post-inoculation, supporting the significant antibacterial activity of the DOPASIL coating (Figure 2b). In support of this, bacterial adhesion to the surface of all coated objects of varying geometries was also prevented (Figure 2c).

Effect of Organic Solvents on DOPASIL Nanoparticle Formation

We further examined the effect of water-miscible organic solvents on the characteristics of in situ formed nanoparticles. We initially utilized dynamic light scattering to measure the hydrodynamic size and the ζ potential of DOPASIL nanoparticles. The hydrodynamic size of the nanoparticles was highly dependent on the water-miscible organic solvent and the solvent/Tris ratio used (Figure 3a). The hydrodynamic size of nanoparticles formed in the absence of the water-miscible organic solvent was determined to be ∼150 nm and decreased as the percentage of MeOH incorporated into the coating solution increased, reaching ∼60 nm for the DOPASIL solution (MeOH/Tris 90:10). Overall, the replacement of a part of Tris buffer with alcohols (MeOH and IPOH) resulted in nanoparticles with much smaller hydrodynamic sizes (Figure S2). The lowest size of the nanoparticles formed in the presence of 90% v/v IPOH could be attributed to the low solubility of DA and inhibited PDA synthesis in IPOH. The larger size of the DMF-synthesized nanoparticles than that of the MeOH-synthesized nanoparticles could be attributed to the higher polarity and DA solubility in DMF, while their oxygen solubility is very close (4×10^{-4} as shown in Table 1). We also showed that the hydrodynamic size of nanoparticles formed in both DOPASIL (MeOH/Tris 90:10 v/v) and SAFE (Tris alone) solutions nearly remained unchanged with time (Figure 3b,c). In contrast, the ζ potential of DOPASIL nanoparticles was not changed with the use of water-miscible organic solvents (Figure 3d). Nanoparticles formed in all solutions containing different solvents and the solvent/Tris ratios were found to be slightly positively charged, which was due to the presence of the positively charged LMW-PEI used in the coating solution. Ag control (MeOH/Tris 90:10 v/v without uhPDMA) nanoparticles were found to be positively charged (∼25 mV) (Figure S3). The decrease in ζ potential of nanoparticles containing uhPDMA can be explained by the presence of uhPDMA chains on the surface of the nanoparticles (also see below).[48] Furthermore, the development of the brown color of the coating solution (an indicator for the extent of DA oxidation/polymerization) was slowed down due to MeOH accounting for 90 vol % of its solvent system (Figure S4). This observation supported our initial hypothesis that the

https://doi.org/10.1021/acsnanoscienceau.2c00040
ACS Nanosci. Au 2023, 3, 67−83

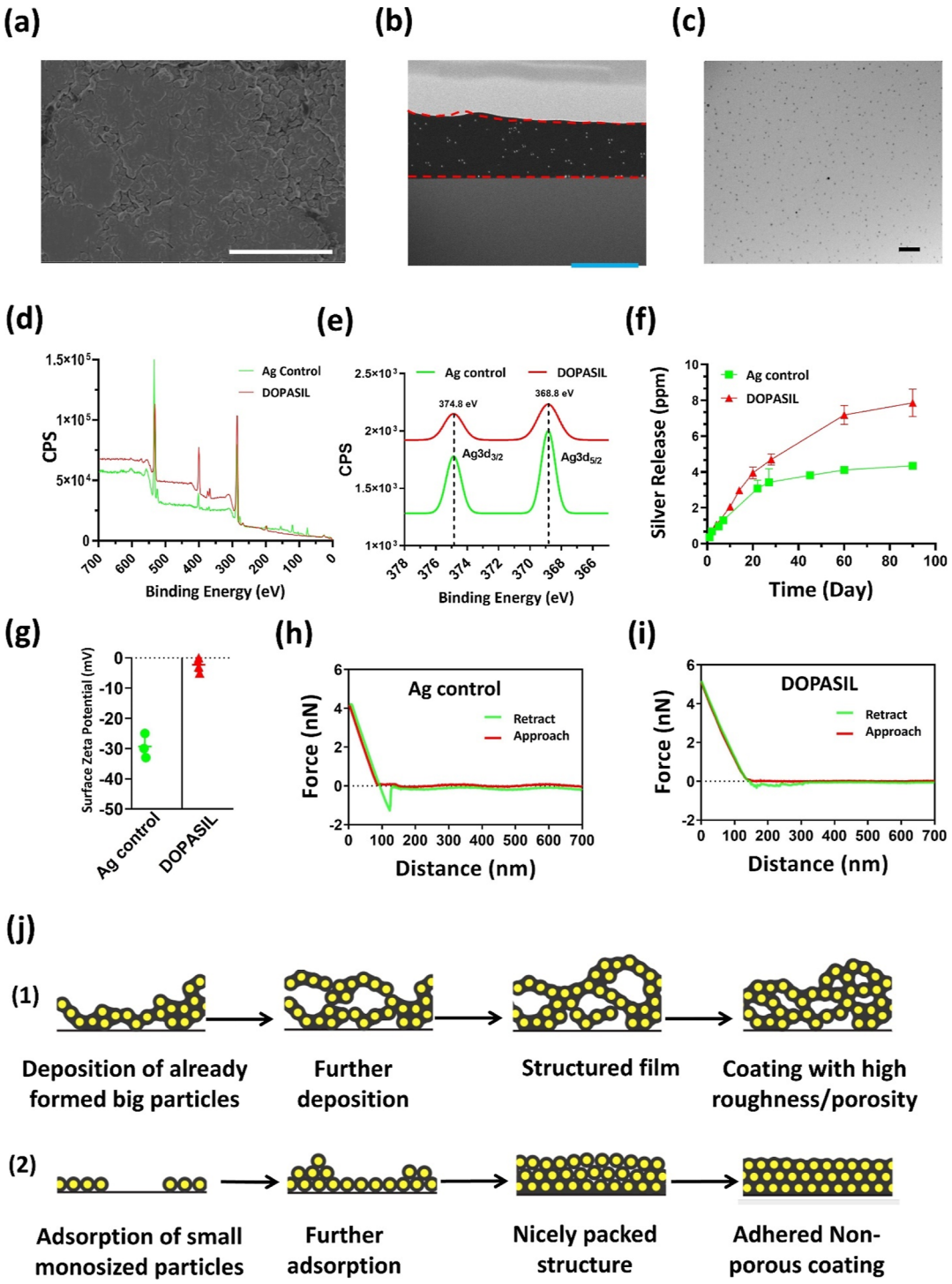

Figure 4. Characterization of the DOPASIL coating. (a) SEM image of the DOPASIL coating. The white scale bar is 5 μm. (b) SEM image of the FIB-created cross section of the DOPASIL coating. The blue scale bar is 2 μm. (c) TEM image of silver nanoclusters incorporated into the DOPASIL coating. The black scale bar is 100 nm. (d) XPS spectra of Ag control and DOPASIL coating. (e) High-resolution XPS spectra of silver for the Ag control coating and the DOPASIL coating. (f) Silver release profile for the DOPASIL coating over 90 days in water. (g) SZP of the Ag control and the DOPASIL coating. Force–distance AFM curves of (h) Ag control and (i) DOPASIL coating on silicon wafer. (j) Cartoon showing the film formation in the absence (1) and the presence (2) of MeOH.

introduction of water-miscible organic solvents could slow the oxidation/polymerization of DA.

Surface Characterization of the DOPASIL Coating

The DOPASIL coating generated a nonporous structure (Figure 4a). Both intra- and extra-luminal surfaces of the silicone urinary catheter were effectively treated with the DOPASIL coating demonstrating its versatility (Figure S5). Focused ion beam-SEM (FIB-SEM) was utilized to determine the thickness of the DOPASIL coating. A cross section of the sample was initially created using FIB, and subsequent SEM imaging revealed the DOPASIL coating to be ~2 μm thick which is nearly half of that of the SAFE coating (formed in the

https://doi.org/10.1021/acsnanoscienceau.2c00040
ACS Nanosci. Au 2023, 3, 67–83

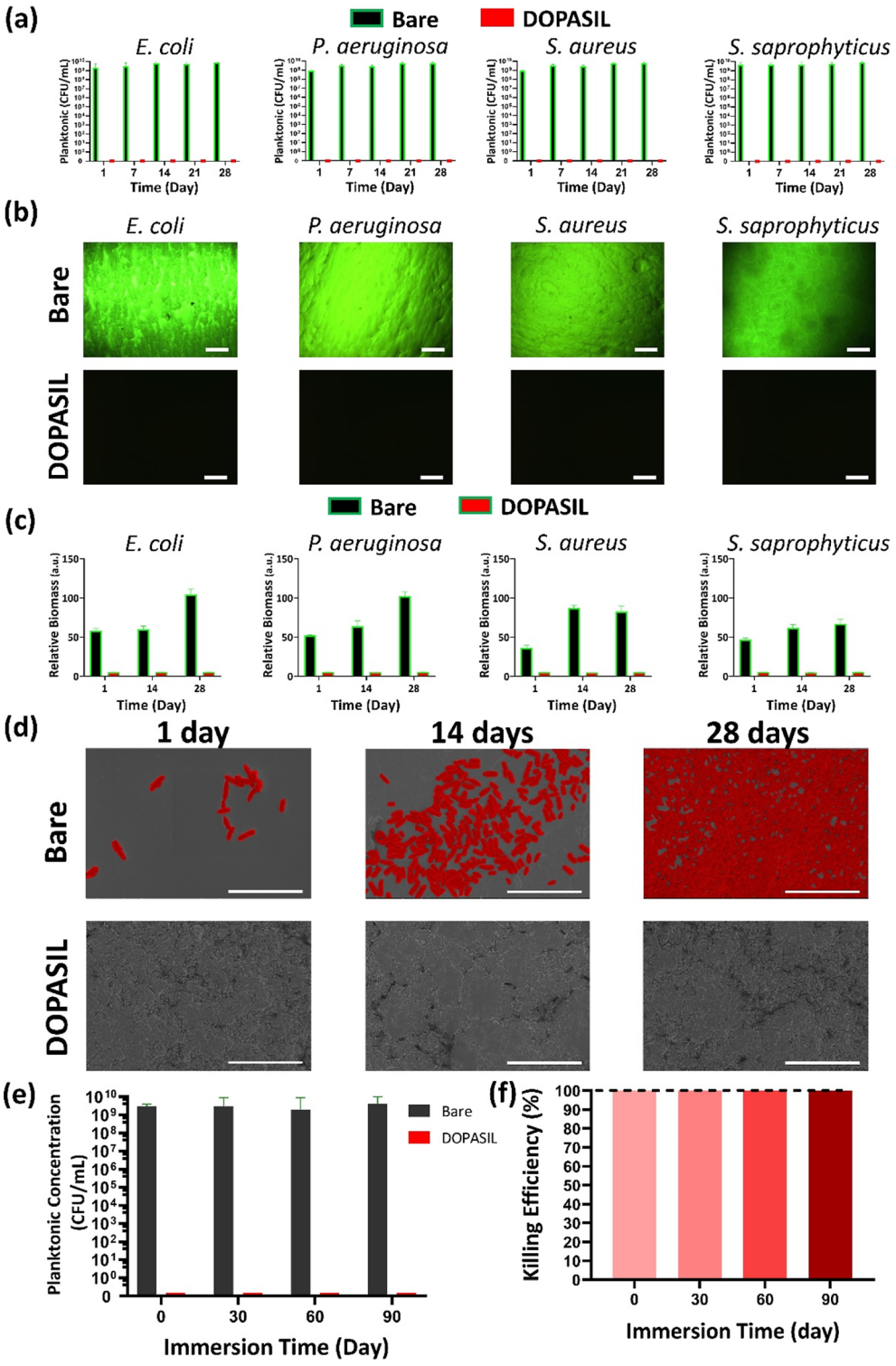

Figure 5. *In vitro* bacteria-killing and anti-adhesive activity of the DOPASIL coating. (a) Planktonic load for the DOPASIL-coated catheter after incubation with diverse bacterial species (1×10^6 CFU/mL, 500 μL) for 24 h. (b) Fluorescence images (green—live bacteria, red—dead bacteria) of biofilm formation and (c) the amount of corresponding biomass deposited on the surface of the uncoated PU sheet and the DOPASIL coating after 28 days of incubation with diverse bacterial strains (1×10^6 CFU/mL, LB, 500 μL). The scale bar is 100 μm. (d) SEM images of biofilm formation on the surface of uncoated and DOPASIL-coated silicone urinary catheters by *E. coli* (initial concentration: 1×10^6 CFU/mL). Surface-attached bacteria are highlighted in red. The scale bar is 10 μm. Number of bacterial colonies attached to the surface of the uncoated and DOPASIL-coated silicone urinary catheters exposed to challenging conditions including (e) number of *E. coli* (initial concentration: 5×10^5 CFU/mL, 500 μL, LB, 24 h) grown in the media with the uncoated or DOPASIL-coated silicone catheter piece already immersed in water for 30, 60, and 90 days. (f) KE of DOPASIL-coated silicone catheter pieces (1 cm) immersed in water for different periods including 0, 30, 60, and 90 days against *E. coli* (500 μL, 5×10^5 CFU/mL, LB, 24 h).

https://doi.org/10.1021/acsnanoscienceau.2c00040
ACS Nanosci. Au 2023, 3, 67−83

absence of MeOH) (Figures 4b and S6). The lower thickness of the DOPASIL coating could be attributed to the decrease in the rate of nanoparticle formation and self-assembly process with the use of MeOH.

Next, we utilized transmission electron microscopy (TEM) to assess the dry size of the nanoparticles. The TEM results showed the SAFE nanoparticles (formed in the absence of an organic solvent) to be assembled into a larger particle (100−200 nm) (Figure S7a), which was not observed for DOPASIL. Instead, the DOPASIL solution was found to consist of well-dispersed individual nanoparticles (∼10 nm) (Figure 4c). Overall, the use of MeOH prevented the formation of assemblies/large particles. The small size of DOPASIL nanoparticles could be attributed to the stabilization effect of uhPDMA assembled on the surface.[17,29,48] The inhibition of large assemblies'/particles' formation in the DOPASIL solution could be attributed to the inhibition effect of MeOH on nanoparticle formation/growth as discussed earlier.

Next, we employed X-ray photoelectron spectroscopy (XPS) to demonstrate the presence of silver within the DOPASIL coating. The XPS analysis confirmed the effective incorporation of silver into both Ag control and DOPASIL coating indicated by the characteristic peak at ∼375 eV corresponding to the Ag $3d_{3/2}$ orbital (Figure 4d,e). We also utilized XPS to investigate the surface coverage of the DOPASIL coating on silicon wafer. The silicon peak (∼155 eV) was not observed in the XPS spectrum of the DOPASIL coating, while it was observed in the Ag control. These data further support the full surface coverage of silicon wafer with the DOPASIL coating. Next, we assessed the silver cumulative release profile for the DOPASIL coating (Figure 4f). The DOPASIL coating was found to slowly release silver ions for 90 days at therapeutic doses (∼9 ppm), known to be nontoxic to human cells.[49,50] This sustained silver release behavior can be explained based on the uniform distribution of small silver nanoparticles within the coating as discussed earlier. In fact, the small nanoparticles provide a considerable surface area for sustained silver dissolution.

We further evaluated the wettability of the DOPASIL coating on silicon wafer. The DOPASIL coating showed a water contact angle (WCA) value of ∼20° which is much lower compared to that of the PDA-alone (∼50°) and Ag control (∼35°) (Figure S7b). The higher hydrophilicity of the DOPASIL coating compared to that of controls could be attributed to the presence of highly hydrophilic uhPDMA chains within the coating. The significant difference in WCA of the PDA-alone and the Ag control coatings was due to the presence of hydrophilic LMW-PEI in the Ag control.

Next, we utilized surface ζ potential (SZP) measurements to probe the surface charge of the DOPASIL coating deposited on the surface. The SZP of the DOPASIL coating was nearly zero, while the Ag control surface was negatively charged. The data suggest that the surface charge of the deposited nanoparticles is fully screened in the presence of uhPDMA (Figure 4g). The SZP data were supported by the surface composition analysis *via* XPS and hydrophilicity by the WCA measurement. The presence of uhPDMA on the surface of the DOPASIL coating was further investigated using atomic force microscopy (AFM) measurements. Two key parameters, the adhesive force and rupture distance, were utilized to confirm the presence of uhPDMA on the surface. The adhesive force on the DOPASIL-coated surface was found to be much lower than that of the Ag control coating, demonstrating a significant decrease in the interaction between the AFM tip and the coated surface in the presence of uhPDMA. The rupture distance of the DOPASIL coating was also determined to be much longer than that of the Ag control coating. The stretched length of the polymer chains or loops by the AFM tip was determined to be ∼300 nm (Figure 4h,i). Both lower adhesive force and longer rupture distance of the DOPASIL coating together demonstrated the enrichment of uhPDMA chains on the surface of the DOPASIL coating.[9,29,48]

We further studied the film formation during the DOPASIL coating deposition. As demonstrated earlier, the particle aggregation was suppressed in the presence of MeOH, which could be due to the limited hydrophobic interactions between the nanoparticles in MeOH or the decrease in hydroxide concentration to catalyze oxidative polymerization reactions.[46,51] We utilized SEM to investigate the morphology of the surface treated with the DOPASIL solution at two different time points (Figure S8). The substrate treated with the DOPASIL solution was covered with small nanoparticles after 4 h. The underlying surface was fully buried with a uniform layer through further assembly of nanoparticles in 12 h. In the absence of MeOH, the in situ formed nanoparticles readily form large assemblies (∼200 nm) (Figure S7a) in the early stage due to the high reactivity of PEI toward PDA. In the presence of MeOH, the slow formation/growth of nanoparticles in solution allows for proper organization of nanoparticles on the surface with time to generate a coating with a dense structure (Figure 4j).

Long-Term Antibiofilm Activity of the DOPASIL Coating

We further investigated the antibiofilm activity of the DOPASIL coating against both Gram-positive and -negative bacteria including *Escherichia coli* (*E. coli*), *Pseudomonas aeruginosa* (*P. aeruginosa*), *Staphylococcus aureus* (*S. aureus*), and *Staphylococcus saprophyticus* (*S. saprophyticus*) up to 28 days. The DOPASIL-coated and uncoated silicone urinary catheters were incubated with bacteria (initial concentration of 1×10^6 CFU/mL, LB, 500 μL). Every 24 h, half of the media was replaced with a fresh bacterial solution for the entire 28 day incubation period to ensure maximal bacterial challenge at all times. Every 7 days, the number of bacterial colonies present in solution was determined. These results show that the DOPASIL coating was highly effective in overcoming the challenging conditions posed by the daily addition of fresh bacteria and eradicated all planktonic bacteria over the entire 28 day duration of the experiment (Figure 5a). This result was consistent for all bacterial species tested. The high antibacterial efficacy of the DOPASIL coating can likely be attributed to the long-term sustained release of silver at therapeutic levels from the DOPASIL coating.

Next, we investigated the biofilm formation on the DOPASIL coating using a live-dead assay over 28 days. The DOPASIL-coated and uncoated PU sheets were treated with different bacterial species as per the same procedure mentioned above (500 μL, LB, 1×10^6 CFU/mL). The samples were washed with sterile PBS, treated with a fluorescent dye kit (propidium iodide and SYTO9), and visualized using fluorescence microscopy. Fluorescent images of 28 day biofilm experiments with different bacterial species are shown in Figure 5b, with values pertaining to biomass accumulation shown in Figure 5c. The DOPASIL coating showed excellent long-term resistance to biofilm formation with no bacteria visible on the coated surface on day 28 of the

https://doi.org/10.1021/acsnanoscienceau.2c00040
ACS Nanosci. Au 2023, 3, 67−83

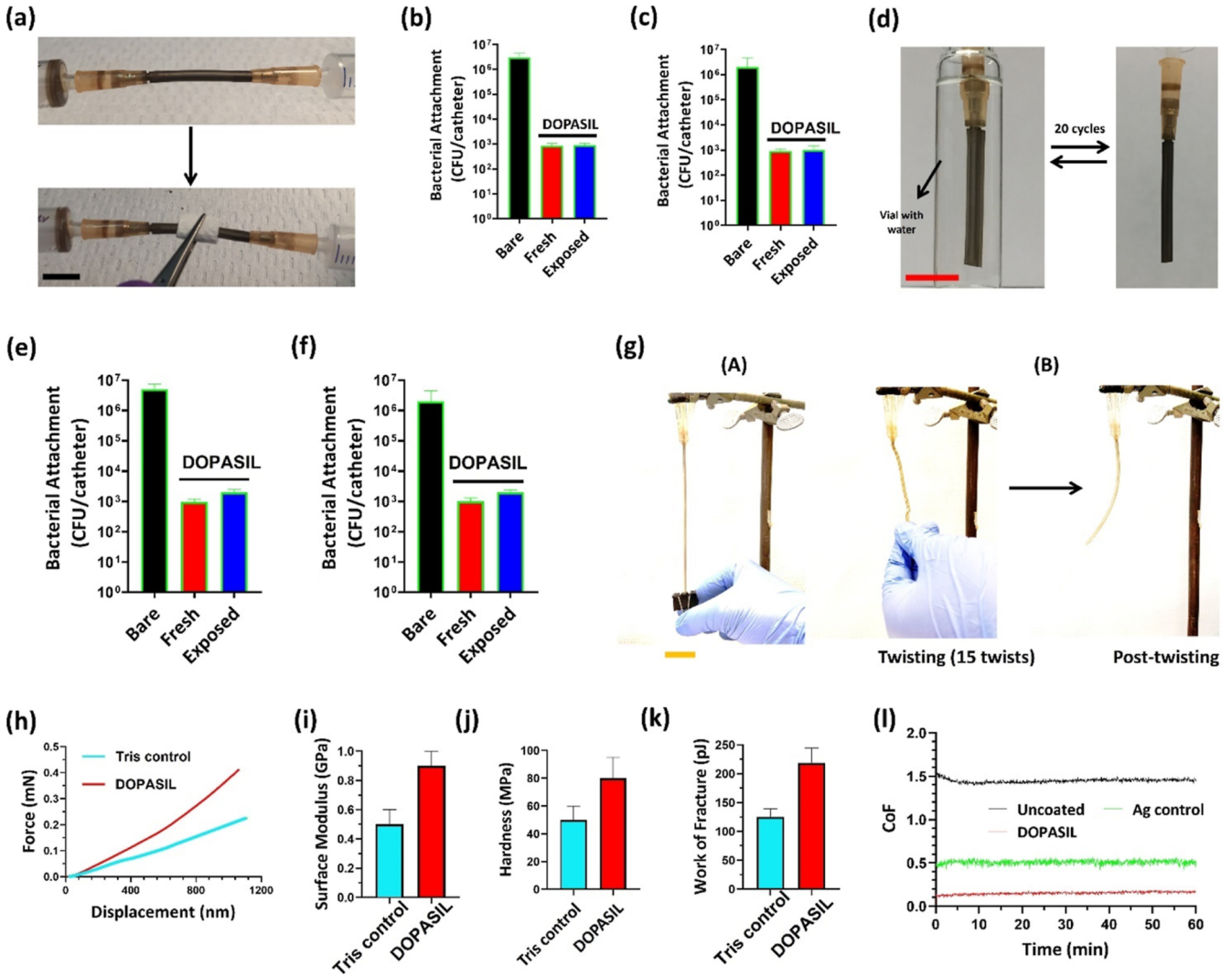

Figure 6. Stability and mechanical properties of the DOPASIL coating. (a) Digital images of the rub-out test setup. The scale bar is ∼1 cm. Antibacterial activity of the (b) rubbed (50 times back and forth) and (c) autoclaved (1 h, 121 °C, 15 psi) DOPASIL-coated silicone urinary catheter (*E. coli*, 1 × 10^9 CFU/mL, 500 μL, 7 days). (d) Digital image of the hydration/dehydration cycle setup. The scale bar is ∼1 cm. Antibacterial activity of the I hydrated/dehydrated (20 cycles) and (f) sonicated (0.5 h in water) DOPASIL-coated silicone catheter (*E. coli*, 1 × 10^9 CFU/mL, 500 μL, 7 days). (g) Digital images of the DOPASIL-coated silicon catheter exposed to different mechanical stresses including stretching (50 stretch−release cycles) and twisting (15 twists). The yellow scale bar is 4 cm. (h) Nanoindentation curves of the DOPASIL coating and the coating formed in the absence of MeOH (Tris control) on silicon wafer. (i) Surface elastic modulus, (j) hardness, and (k) work of fracture of coatings formed on PU sheets. (l) CoF between coated PDMS balls and the uncoated PDMS sheet.

experiment for all the species tested. In contrast, the uncoated surface showed a thick biofilm over the same period.

We also confirmed the anti-adhesive performance of the DOPASIL-coated silicone urinary catheter utilizing SEM. The SEM results showed that the bacterial attachment to the surface of the uncoated catheter increased with time, while the DOPASIL coating prevented the deposition of bacterial biomass onto the surface over the long term (28 days) (Figures 5d and S9). Both the high bactericidal activity of released silver ions and excellent antifouling performance of uhPDMA worked in synergy to make the surface of the DOPASIL-coated silicone catheter highly resistant to bacterial attachment and maintained a clean surface over the 28 day experimental period.

We next assessed the long-term stability and activity of the DOPASIL coating following long-term exposure of 1 cm catheter pieces to water (37 °C) with constant stirring for 90 days. At different time points (30, 60, and 90 days), the catheter piece was taken out, and its bacteria-killing activity was tested in the presence of *E. coli* (initial concentration: 5 × 10^5 CFU/mL, 500 μL, LB, 24 h). We showed that the DOPASIL-coated catheter retains its excellent bacteria-killing activity [100% killing efficiency (KE)] even after 90 days of immersion in water, while there was a high load of planktonic bacteria in the solution in which the bare catheter was incubated (Figure 5e,f).

Cell Adhesion and Protein Binding to the DOPASIL Coating

We further assessed the biocompatibility of the DOPASIL coating *in vitro*. We investigated the adhesion of bladder cells (T24) onto the DOPASIL-coated cell culture slides (glass) over a 24 h period. The DOPASIL coating effectively prevented cell adhesion, whereas the Ag control showed some cell attachment to the surface (Figure S10a). This clear difference in the cell attachment of the two coatings confirmed

https://doi.org/10.1021/acsnanoscienceau.2c00040
ACS Nanosci. Au 2023, 3, 67−83

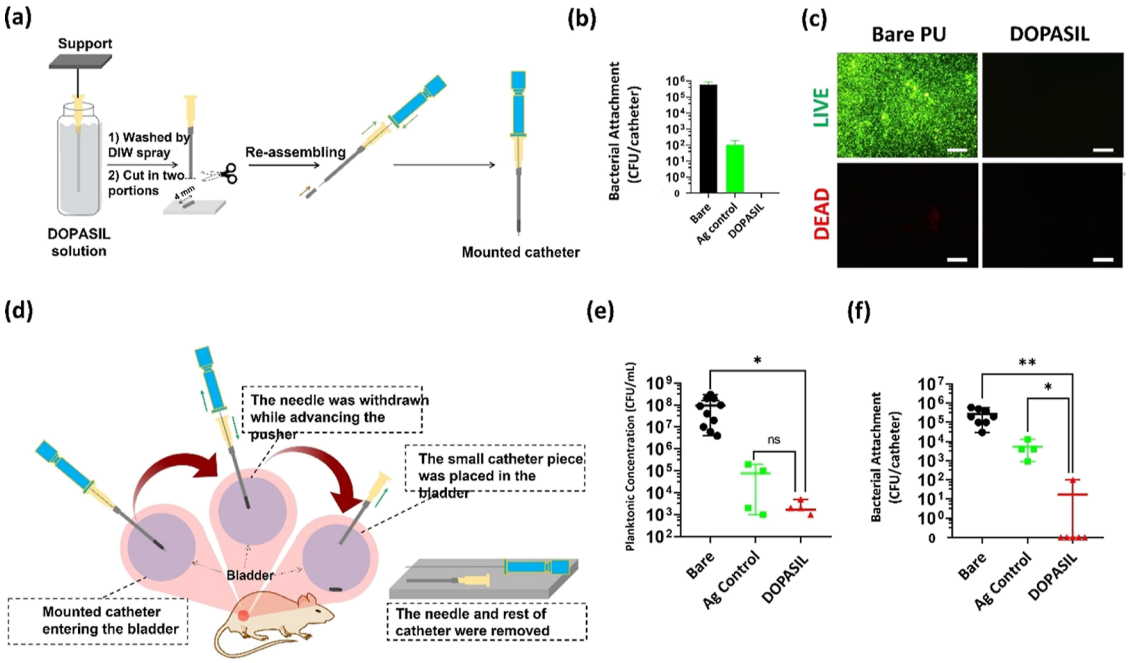

Figure 7. *In vivo* infection prevention efficacy of the DOPASIL coating. (a) Cartoon of DOPASIL surface modification of 24G IV PU catheters. (b) Number of bacterial colonies attached to the surface of the uncoated, Ag control-coated, and DOPASIL-coated pieces of the 24G IV PU catheter (4 mm long) after 3 days of incubation with *P. mirabilis* (1×10^6 CFU/mL, 500 μL, artificial urine). (c) Fluorescence images of biofilm formation on the surface of uncoated and DOPASIL-coated PU sheets after 3 days of incubation with *P. mirabilis* (1×10^6 CFU/mL, 500 μL, artificial urine). The scale bar is 100 μm. (d) Implantation of the small portion of the catheter: the mounted catheter was pushed inside to ensure that the whole small portion gets in. The needle was withdrawn while keeping the large portion penetrated into the bladder. Finally, the large portion was withdrawn, and the small portion was dropped inside. (e) Number of planktonic bacteria present in the bladder of mice treated with *P. mirabilis* (concentration of the injected bacterial solution: 5×10^5 CFU in 50 μL PBS) for 3 days. (f) Number of bacterial colonies attached to the surface of uncoated, Ag control-coated, and DOPASIL-coated pieces of 24G PU IV catheters after 3 days of implantation with *P. mirabilis* (concentration of the injected bacterial solution: 5×10^5 CFU in 50 μL PBS). * indicates *P* value $\leq$ 0.05, and ** indicates *P* value $\leq$ 0.01. ns shows not statistically significant.

the strong antifouling and high biocompatibility properties of the DOPASIL coating. To expand the assessment of antifouling activity further, we also assessed the protein deposition on the surface of the DOPASIL coating using fluorescein thioisocyanate-tagged bovine serum albumin (FITC-BSA). Serum albumin was chosen based on the fact that it is a major component of the urinary conditioning film found on indwelling urinary devices in contact with urine.[52,53] There was no detectable protein deposition observed on the surface of the DOPASIL coating, while the Ag control coating was fully covered with the protein (Figure S10b). Taken together, the data demonstrated the superior antifouling and biocompatibility properties of the DOPASIL coating. Since the antifouling activity of the DOPASIL coating is so efficient that it effectively repels cells, we could not perform the conventional cell viability studies with adherent cell lines. That said, based on the silver release data discussed earlier, the average amount of silver ions released per 24 h is much lower than the toxic range reported for silver ions and silver nanoparticles, which is consistent with the nontoxicity of the DOPASIL coating.[49]

Durability of the DOPASIL Coating

One of the challenges of the silver-based coating is its poor mechanical properties and stability. Thus, we investigated the stability of the DOPASIL coating following exposure to different harsh conditions. The stability tests included a rub-out test (50 times back and forth runs) (Figure 6a), autoclaving for 1 h, sonication for 0.5 h, and 20 hydration/dehydration cycles. After these mechanical challenges, the anti-adhesive property of the exposed coating was investigated and compared with that of the freshly made DOPASIL-coated and uncoated catheters following 7 days of incubation with *E. coli* (500 μL, LB, 1×10^6 CFU/mL). The DOPASIL coating retained its excellent bacteria-repelling activity even after exposure to 50 rubbing cycles (Figure 6b). In fact, the anti-adhesive performance of the rubbed DOPASIL coating was similar to that of the fresh DOPASIL coating. Similarly, exposure of the DOPASIL coating to a 1 h autoclave cycle (elevated temperature and high pressure) showed the same high anti-adhesive activity as a freshly made DOPASIL coating (Figure 6c). To simulate a hydration/dehydration cycle, DOPASIL-coated and uncoated samples were allowed to rehydrate for 24 h in water followed by overnight dehydration on the benchtop (experimental setup shown in Figure 6d). This process was repeated 20 times to examine the stability of the coating to repetitive hydration/dehydration cycles. Overall, the anti-adhesive activity of the DOPASIL coating remained unchanged even after 20 cycles (Figure 6e). Similarly, sonication for 0.5 h did not change the superior antibacterial and anti-adhesive activity of the DOPASIL coating (Figure 6f). In addition to testing the anti-adhesive activity, we assessed the morphology of the coating after exposure to different stability tests and compared to that of the freshly made DOPASIL coating. Exposure of the DOPASIL coating to any of the harsh conditions described did not significantly change the overall morphology demonstrating an overall high level of stability (Figure S11). We further assessed the durability of the

https://doi.org/10.1021/acsnanoscienceau.2c00040
ACS Nanosci. Au 2023, 3, 67−83

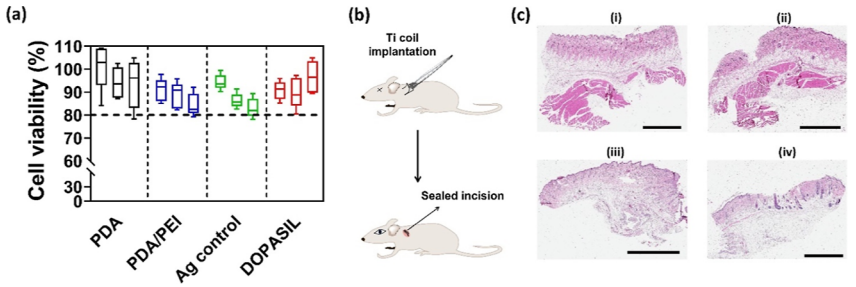

Figure 8. Biocompatibility of the DOPASIL coating. (a) *In vitro* cytotoxicity of different coatings including PDA, PDA/PEI, Ag control, and DOPASIL. The viability of T24 cells in media [RPMI, 10% FBS, 1% (P/S)] incubated with the coatings for 12 h (left box), 24 h (middle box), and 48 h (right box) was measured after 24 h of culture. The experiment was done using media released from five independent samples in each coating group. (b) Cartoon showing the insertion of the Ti implant under the skin on the back of the rat in the subcutaneous pocket. (c) Optical microscopy images of the H&E-stained section of (i) healthy skin tissue and skin tissues in vicinity of the (ii) uncoated Ti implant, (iii) Ag control-coated Ti implant, and (iv) DOPASIL-coated Ti implant. The scale bar is 2 mm.

DOPASIL coating (Figure 6g) by exposing a DOPASIL-coated 10 Fr silicone catheter to different mechanical stresses including stretching (50 stretch−release cycles) and twisting (15 twists), followed by a qualitative/visual assessment for any coating defects/detachments. Overall, we did not observe any coating delamination post-stretching and no coating material transfer to the glove post-twisting. The DOPASIL coating retained its excellent antibacterial efficacy post-stretching/twisting (the antibacterial efficacy was tested against *E. coli* with a starting concentration of 1×10^6 CFU/mL and an incubation time of 24 h; we noticed all bacterial cells to be killed within 24 h by the DOPASIL coating experienced iterative stretches/twists). Taken together, the above results indicate the great durability of the DOPASIL coatings when exposed to different environments and mechanical stresses.

Next, we quantitatively characterized the mechanical properties of the DOPASIL coating utilizing nanoindentation measurements. The force−displacement curves of different coatings prepared on silicon wafer were collected for the determination of surface elastic modulus and hardness (Figure 6h). The surface elastic modulus of the DOPASIL coating was found to be nearly 2 times greater than that of the SAFE coating (the coating formed in the absence of MeOH) (Figure 6i). The hardness data showed that the DOPASIL coating was harder than the SAFE coating (Figure 6j). In addition, the work of fracture calculated from the area under the force−displacement curve which represents the mechanical toughness of the coating was higher for the DOPASIL coating (Figure 6k). Taken together, the DOPASIL coating was found to be tougher than the SAFE coating, demonstrating the positive impact of MeOH on the increased mechanical stability of the DOPASIL coating. The improved mechanical properties of the DOPASIL coating compared to the coating formed in the absence of MeOH may be attributed to the dense structure of the DOPASIL coating due to slower nanoparticle deposition. In addition, the presence of inorganic silver nanoparticles that can act as a nanofiller could be the reason for high toughness of the DOAPSIL coating.[54,55] The effective dispersion of silver nanoparticles in the PDA/polymer matrix in DOPASIL coating could result in high energy dissipation as the mechanical stress is applied in comparison with the control coatings.

We further investigated the lubrication properties of the DOPASIL coating utilizing tribometry measurements. The coefficient of friction (CoF) between the coated PDMS ball and the uncoated flat PDMS sheet was collected over 60 min. The CoF of the DOPASIL-coated PDMS ball was ∼0.1 which was much lower than that of the Ag control (without uhPDMA) coated (∼0.5) and uncoated ball (1.5) (Figure 6l), indicating that the lubricity of the DOPASIL coating is greater, which is attributed to the enrichment of uhPDMA chains on the material surface.

In Vivo Antibiofilm Efficacy of the DOPASIL Coating in Mice

To assess the translation of the significant characteristics of the DOPASIL coating assessed above into a preclinical *in vivo* model, we examined the efficacy of the DOPASIL coating to prevent bacterial adhesion and biofilm formation on indwelling catheters using a mouse model of catheter-associated urinary tract infection.[9] For this, we utilized coated and uncoated 24G IV PU catheters. The catheters were coated with the DOPASIL composition *via* a simple dip-coating process as shown in Figure 7a. The catheter was cut in two portions including the small (4 mm long) and large portions, followed by reassembling on the needle to form a mounted catheter (Figure 7a). To truly challenge the DOPASIL coating, we chose to assess its activity against *Proteus mirabilis*, a common uropathogen associated with catheter-associated urinary tract infections. *P. mirabilis* is considered a complicated pathogen as it causes ascending (enter the kidneys) infections and, *via* the expression of urease, is associated with the formation of crystalline layers that encase and block entire catheters and can form into larger stones that encase the entire collecting system of the kidneys known as staghorn stones.[56] To ensure the activity of the samples before insertion into the animals, we initially investigated the antibiofilm activity of the DOPASIL-coated piece of the catheter (4 mm) against *P. mirabilis* (500 μL, 2×10^6 CFU/mL in artificial urine, 3 days) *in vitro*. There were no bacteria detected on the surface of the DOPASIL-coated catheter, while a large number of colonies were found on the surface of uncoated catheters (Figure 7b). The live-dead assay further confirmed that the DOPASIL coating on the PU sheet effectively prevents biofilm formation by *P. mirabilis* (Figure 7c). Following verification of antibacterial and anti-adhesive activities *in vitro*, a small portion of the same catheter was implanted into the mouse bladder (Figure 7d). *P. mirabilis* (2×10^6 CFU in 50 μL of PBS) was injected into the mouse bladder, and animals were recovered for 3 days at which point planktonic bacteria in urine and adherent bacteria on the catheter were assessed *via* CFU counts. Even in the *in vivo* environment, the DOPASIL coating showed remarkable KE of planktonic (free swimming in urine) and adherent bacteria to the catheter surface. Overall, the presence of the coating

https://doi.org/10.1021/acsnanoscienceau.2c00040
ACS Nanosci. Au 2023, 3, 67−83

resulted in a 5 log reduction in the number of bacteria in the urine compared to that in animals that had the Ag control catheter inserted (Figure 7e). Similarly, a ∼5 log reduction in bacteria adhered to the surface of coated catheters was observed (Figure 7f). Collectively, these data indicate that the superior antibacterial and anti-adhesive properties of the DOPASIL coating observed in the *in vitro* setting translate directly to a more realistic *in vivo* environment of catheter-associated urinary tract infection. This very much speaks to the potential effectiveness of this coating technology to reduce device-associated infections in humans.

Biocompatibility of the DOPASIL Coating

We next assessed the biocompatibility of the DOPASIL coating *in vitro* and *in vivo*. As mentioned above, given the significant antifouling activity of the coating, we are unable to perform cell adhesion studies to assess direct toxicity of the coating. As a result, we evaluated the potential toxicity of silver ions released from the DOPASIL coating. To that end, the coated PU coupons (5 × 5 mm) were incubated with cell culture media [Roswell Park Memorial Institute (RPMI), 10% fetal bovine serum (FBS), 1% penicillin/streptomycin (P/S)] for different time periods (12, 24, and 48 h), and the collected supernatant was used to assess cell growth (T24 bladder cells). The biocompatibility of both silver-free (PDA and PDA/PEI) and silver-containing controls (Ag control) was shown to be high, with >90 and >80% cell viability, respectively. In comparison, the cell viability for the DOPASIL coating was also found to be >90% irrespective of the time point taken supporting the high biocompatibility of the coating (Figure 8a). To determine how this translates to an *in vivo* environment, we utilized a subcutaneous implantation model in rats. For this, DOPASIL, Ag control, and uncoated Ti coils were implanted into two dorsal pockets on the animals, followed by suturing of the incision and recovery of the animals for 7 days (Figure 8b). After 7 days, the tissue around the implants was harvested and histologically examined after staining with hematoxylin and eosin (H&E) in a blinded fashion by a board-certified pathologist. Results show that there were no significant differences in the tissue responses to either the Ag control or the DOPASIL coating (Figure 8c); the immune cell infiltration and tissue damage were similar to that of the uncoated Ti implants. The high biocompatibility of the DOPASIL coating can be attributed to the surface enrichment of biocompatible PDMA on the surface and the sustained release of nontoxic yet therapeutic levels of silver. While the Ag control sample is not covered by a highly biocompatible PDMA layer, the amount of silver ions released is minimal, resulting in low toxicity and good biocompatibility (see Figure 8ciii). Overall, the normal healing process following the surgical procedure was evident from the presence of mild inflammatory infiltrate in the dermis and hypodermis for all implant groups. We also noticed some inflammatory reactions typical for a foreign body-type reaction in some tissue specimens which is expected given the fact that a foreign material was implanted. Taken together, these data further support the high biocompatibility of the DOPASIL coating and are consistent with our *in vitro* cell adhesion and cytotoxicity experiments using T24 urinary bladder cells.

DISCUSSION

One of the major complications associated with the implantation of medical devices in clinics and hospitals is the biofilm formation that can trigger local and systemic infection which is difficult to treat.[5,6] One approach to prevent such an infection is to endow the medical devices with a robust surface on which biofilm formation fails. However, the surface modification of commercially available medical devices that are designed to be nonadhesive to microorganisms, kill microorganisms, and prevent biofilm formation remains challenging.[2,4,57] Hydrophobicity and lack of reactive functional groups on the surface of such materials (e.g., silicone) limit the effective interaction between the surface and coating materials. The current study reported the development of a robust nanoparticle-derived coating with combined antifouling and antibiofilm with long-term broad-spectrum activity applicable to the surface of diverse materials. We demonstrated that the coating can be effectively applied to a range of polymeric catheters and other objects irrespective of the size, geometry, and surface chemistry. The control of nanoparticle stabilization using an ultra-high-molecular-weight hydrophilic polymer and a water-miscible organic solvent in combination with silver generated an easy-to prepare scalable coating (through a one-step dip-coating process at room temperature) which is uniform has excellent mechanical properties and outstanding antibiofilm activity. The optimal coating gave sustained release profiles of silver over long time periods (∼90 days) at effective doses and fully inhibited bacterial growth in the solution and on the surface irrespective of the bacterial strain studied. This opens up the possibility of treatment in the case of device-associated infections by replacing the infected device with the DOPASIL-coated device. This coating was highly lubricious and showed great scratch resistance and adhesion to hard-to-coat materials such as silicone. The anti-adhesive and bactericidal activity of the coating resulted in superior antibiofilm activity as evidenced by a 5 log reduction in *P. mirabilis* in both urine and adherent to the catheter surface on DOPASIL-coated catheters *in vivo*. Given the significant efficacy of this coating along with the ease of application to difficult-to-treat medical devices with intricate geometry through a simple process, this coating has significant potential to be a game changer in areas and applications where the reduction of surface fouling and bacterial biofilm formation to prevent material failure is a top priority. This includes medical-device-associated infections which is one of the leading causes for hospital-acquired infections globally. To further demonstrate this, additional studies are needed to evaluate the efficacy of this coating utilizing infection models in larger animals (e.g., a urinary tract infection model in pigs) in the future.

EXPERIMENTAL SECTION

Materials

Allylamine, MeOH, EtOH, IPOH, DMF, DMSO, DA hydrochloride, silver nitrate, and LMW-PEI (700 Da) were purchased from Sigma. PDMA (uhPDMA, 900 kDa) was synthesized based on the procedure which was previously developed in our lab.[48] The PU sheet was purchased from Professional Plastics. The polymeric catheters including Foley catheters, 24G PU IV, 10 Fr silicone urinary, and 16 Fr PVC urinary catheter were supplied by BD. The PDMS sheets were cast in the lab using reagents purchased from Dow Corning. All cell culture-related media and supplements [trypsin−EDTA, Dulbecco's phosphate-buffered saline (DPBS), heat-inactivated FBS, P/S, RPMI 1640 medium, modified eagle medium, and MeOH] were received from Thermo Fisher Scientific unless otherwise specified. T24 bladder carcinoma cells were purchased from American Type

https://doi.org/10.1021/acsnanoscienceau.2c00040
ACS Nanosci. Au 2023, 3, 67−83

Culture Collection (ATCC CRL-2922 Manassas, VA) and were used between passage numbers 5 and 10.

Coating Synthesis

Organic Solvent Containing Solutions. uhPDMA (35 mg) was dissolved in a mixture (7 mL) of solvent (MeOH, EtOH, IPOH, DMF, and DMSO) and Tris (10 mM, pH 8.5) at different ratios. Afterward, LMW-PEI (10.5 mg), silver nitrate (3.5 mg), and DA (14 mg) were added to the uhPDMA solution. The solution was vortexed for 10 s.

DOPASIL Solution. uhPDMA (35 mg) was dissolved in a mixture of solvent (i.e., MeOH; 6.3 mL) and Tris (10 mM, pH 8.5; 0.7 mL). Afterward, LMW-PEI (10.5 mg), silver nitrate (3.5 mg), and DA (14 mg) were added to the uhPDMA solution. The solution was vortexed for 10 s.

SAFE Solution. uhPDMA (35 mg) was dissolved in Tris (10 mM, pH 8.5; 0.7 mL). Afterward, LMW-PEI (10.5 mg), silver nitrate (3.5 mg), and DA (14 mg) were added to the uhPDMA solution. The solution was vortexed for 10 s.

Ag Control Solution. LMW-PEI (10.5 mg), silver nitrate (3.5 mg), and DA (14 mg) were dissolved in the MeOH/Tris solution with a volume ratio of 90:10 [6.3 mL of MeOH and 0.7 mL of Tris (10 mM) at pH 8.5] in order.

The oxygen plasma-treated catheters were placed in the resulting coating solutions. Oxygen plasma (M4L Plasma Processing System from PVA Tepla) was utilized to pretreat the surface of different objects according to a procedure reported previously.[9] To prepare different coatings (DOPASIL, Ag control, and SAFE), the plasma-pretreated objects were vertically suspended in glass vials containing the relevant coating solutions at room temperature for 24 h. The volume of the PDA solution used was different for different objects (Table S1). Then, the coated objects were taken out and sprayed thoroughly with deionized water, washed with water, and then stored in air at room temperature (22 °C) for further analysis.

To coat flat surfaces (silicon wafer and PU sheets), a piece of the sample (5 × 5 mm) was cut and placed in the well (48-well plate) containing the relevant coating solution (500 μL) at room temperature for 24 h. Then, the samples were taken off and rinsed thoroughly with deionized water, washed with water, and then stored in air at room temperature (22 °C) for further analysis.

WCA Measurements

We utilized a home-made setting for the measurement of WCA. The digital camera installed was Retiga 1300 (Q-imaging Co). The volume of the water droplet used was 4 μL. The WCA of three spots on each sample was recorded. The average of three WCAs was reported.

Scanning Electron Microscopy

The Helios filed-emission scanning electron microscope was employed for SEM imaging. The accelerating voltage was 1 kV. The sample was bound to the aluminum SEM stubs utilizing double-sided carbon conductive tapes. The sample was mounted with silver paint, followed by coating with a thin layer of iridium (Ir) (20 nm) by a Leica sputter coater. The sputtering parameters included working distance (3 mm) and current (80 mA). We also utilized energy-dispersive X-ray accessory equipped on the SEM instrument. The acceleration voltage used for EDAX measurements was 10 kV. The same sample was etched by FIB to create cross section. The SEM image of the FIB-created cross section was taken.

Transmission Electron Microscopy

The FEI Tecnai F20 TEM/STEM microscope was used for TEM imaging at 100 kV. To prepare samples, the coated silicon wafer was scraped off using a keen blade. The coating material was sonicated in EtOH for 15 min to disperse nanoparticles. A droplet of the sonicated solution was placed on copper grids with an ultrathin carbon film on a lacey carbon support film. Prior to imaging, the grids were kept for ∼30 min to dry off EtOH.

Atomic Force Microscopy

A Nanoscope IIIa controller (Digital Instruments, Santa Barbara, CA) was used to record AFM force−distance curves. The scan size was 130 × 130 μm^2. The AFM tip (NP-S10, Veeco) used was a V-shaped cantilever made of silicon nitride. The back side of the cantilever used is coated with gold for laser reflection. The speed of the tip during approach and retraction was 0.5 mm/s, respectively.

Inductively Coupled Plasma−Optical Emission Spectroscopy

The samples (silver-coated substrates, 5 mm × 5 mm) were immersed in water (1 mL). At different intervals, supernatants were collected. The samples were replenished with fresh water. To prepare samples for inductively coupled plasma−optical emission spectroscopy (ICP−OES), 2% nitric acid solutions (2 mL) were added to supernatants (1 mL). The ICP instrument equipped with a Varian 725ES OES was used.

Dynamic Light Scattering

To prepare samples, the solution (10 μL) was diluted with Tris buffer (990 μL). The samples were transferred to polystyrene cuvettes. Afterward, the cuvette was loaded onto the Zetasizer Nano ZS (Malvern). The hydrodynamic size was measured three times. The average of three measurements was reported. Afterward, the same sample was transferred to the folded capillary cells used for ζ potential measurements. The ζ potential was measured three times. The reported value was the average of three measurements. To prepare samples for SZP measurements, the silver-coated silicon wafer (4 × 5 mm^2) was glued to the SZP probe and placed in the polystyrene cuvette containing 1 mL of the transfer standard suspension (DTS1235). Afterward, SZP was measured using the SZP accessory.

Bacterial Culture (*P. aeruginosa*, *E. coli*, *S. aureus*, and *S. saprophyticus*)

All bacterial species were grown in LB at 37 °C overnight from freezer stocks (−80 °C). On the day of the experiment, the bacterial concentration was determined by measuring the optical density of the bacterial solution at 600 nm. Based on these numbers, fresh bacterial solutions (1 × 10^6 CFU/mL) were prepared by diluting the cultured bacterial solution with LB.

Shaking Experiments

The samples were mounted onto 1.5 mL microtubes, followed by incubating with 70% EtOH (1 mL) for 5 min for sterilization. Afterward, the samples were washed three times by pipetting up and down. The sterilized samples were incubated with 500 μL of bacterial solution (initial concentration: 1 × 10^6 CFU/mL). The samples were kept rotating (using rotary mixers at 18 rpm) in the incubator at 37 °C for 28 days. Each day, half of the media was changed with a fresh bacterial solution (1 × 10^3 CFU/mL) to ensure continuous exposure to freshly growing bacteria. At different time points, the samples and supernatants were collected for planktonic growth and bacterial adhesion analyses. To analyze the activity of the DOPASIL coating on diverse objects, the same procedure was followed except that a different volume of bacterial solution and container was used (Table S1).

Planktonic Growth Analysis

Following co-incubation with coated and uncoated samples, the bacterial suspension was serially diluted to 10^{-8} and spot plated (10 μL spots) onto LB agar plates. Following overnight incubation at 37 °C, colonies were counted, and the bacterial numbers were reported as CFU/mL.

Bacterial Adhesion Analysis

Biofilm Formation Analysis. Samples for biofilm analysis were removed at varying time points and washed five times gently using 1 mL of sterile PBS. The washed samples were then incubated in 500 μL of a SYTO9/PI cocktail (3 μL/mL) for 15 min and washed three times with sterile water (1 mL). The washed samples were imaged utilizing the fluorescence microscope (Zeiss Axioskop 2 Plus, Carl Zeiss Microimaging Inc). SEM was also utilized to examine the biofilm formed on the surface. The samples were taken out from the culture media, followed by washing with sterile PBS as above and fixing with 2.5 wt % glutaraldehyde for 4 h at 4 °C. The fixed samples

https://doi.org/10.1021/acsnanoscienceau.2c00040
ACS Nanosci. Au 2023, 3, 67−83

were dehydrated using an EtOH gradient (50, 60, 70, 80, 90, 95, 100, and 100%) for 10 min each. Further preparation for analysis was performed as described in the SEM section above.

Counting Surface-Attached Bacterial Cells. Samples were taken out and rinsed with sterile PBS as above (1 mL), followed by detachment of bacteria in a sonicating water bath in sterile PBS for 10 min. After sonication, the supernatants were collected and serially diluted with sterile PBS and quantified using the spot plate method described above.

To assess the *in vitro* activity of the DOPASIL-coated 24G IV PU catheters against *P. mirabilis*, catheter portions (4 mm) were placed in wells of a 48-well plate containing a 500 μL solution of *P. mirabilis* in artificial urine.[58] The initial concentration of the *P. mirabilis* solution used was 1×10^6 CFU/mL. Half of the media was replenished with a fresh bacterial solution (1×10^3 CFU/mL) every day. The samples were taken out, washed, and sonicated for 10 min. The supernatants were collected for bacterial analysis using the spot plate method described above.

Stability Measurements

To assess the storage stability of the DOPASIL coating, the coated silicon catheter pieces (1 cm) were stirred for 90 days in water at 37 °C at 150 rpm. The stirred pieces were taken out at different time points (30, 60, and 90 days). The number of planktonic bacteria present in LB incubated with the stirred pieces was determined based on the abovementioned protocol (*E. coli*, 5×10^5 CFU/mL, 24 h).

To investigate the mechanical stability of the coating, coated catheters were exposed to different testing conditions. Then, the morphology and anti-adhesive activity of the exposed samples were compared to those of freshly made samples.

Rub/Scratch Resistance. To assess the scratch resistance of the coating, a piece of the coated catheter (3 cm) was placed between two clamps and rubbed back and forth for 50 times. To investigate the coating resistance to stress developed during hydration/dehydration, the coated catheter (3 cm) was immersed in deionized water for 24 h. Then, the catheter was removed and placed on the benchtop overnight. This process was repeated 20 times. To assess the stability of the coating at elevated temperature and pressure, the coated catheter (3 cm) was placed in an autoclave for 1 h at 121 °C at 15 psi. To evaluate the adhesion of the coating to catheter, the coated catheter (3 cm) was placed in a sonication bath for 0.5 h.

DOPASIL Resistance to Repeated Stretching. The DOPASIL-coated catheter piece (15 cm) was clamped, while one end was free, followed by attaching the free end to a binder clip. The binder clip was expanded nearly 4 cm, followed by retracting to its original length. This cycle was repeated for 50 times. Afterward, the appearance of the coated catheter was assessed in terms of the coating detachment/defects.

DOPASIL Resistance to Twisting. The DOPASIL-coated catheter piece (15 cm) was clamped. The catheter was manually twisted 15 times and released to reach its original situation. Afterward, the appearance of the coated catheter was assessed in terms of the coating detachment/defects.

Tribometry Analysis

A conventional T50 pin-on-disk tribometer (Nanovea, Irvine, CA, US) was employed to measure the friction coefficient of coatings. The speed of the disk rotation was 60 rpm. The wearing radius was 5 mm. The applied force was 2 N. The lubricant was water. The PDMS balls (diameter: 6 mm) were cast using SYLGARD 184 (Dow Corning, Midland, MI, US) reagents (part A/part B = 10:1) in a 3D-printed mold. The casted mold was stored at room temperature for 24 for partial curing, followed by storing at 100 °C for 35 min for full curing. To coat PDMA balls, they were initially treated with oxygen plasma according to our previously used procedure.[9] The pre-treated balls were coated with DOAPSIL using the same DOPASIL preparation procedure as described earlier. The CoF between the coated PDMS ball and uncoated PDMS sheet was measured.

Nanoindentation Measurements

The modulus and hardness of the materials were measured using an MTS DCM nanoindenter. Continuous stiffness measurement in a Berkovich tip was used to measure the elastic modulus and hardness continuously to the penetration depth of 1000 nm at the strain rate of 0.05 s^{-1}. The harmonic displacement target was set as 1 nm at 75 Hz frequency. The elastic modulus and hardness were averaged from the data collected.

Cell Adhesion Experiments

T24 bladder carcinoma cells were cultured in RPMI 1640 medium with 10% FBS and 1% P/S at 37 °C and 5% CO_2. Upon reaching 70% confluence, cells were dissociated with 0.25% trypsin and 0.05% EDTA (Gilco, 25300062), pelleted by centrifugation at 300*g*, and resuspended with complete RPMI-1640 medium. Cells were seeded at 30,000 cells per well in coated/uncoated 8-well tissue culture glass slides and allowed to adhere for 24 h at 37 °C and 5% CO_2. Afterward, the slides were washed three times with cold DPBS and fixed with 4% PFA for 15 min at room temperature in the dark. Fixed cells were stained with nuclear stain, Hoechst 33342 (1:10,000 dilution; Thermo Fisher Scientific). Slides were mounted with a Fluoromount-G mounting medium (SouthernBiotech Birmingham, AL). Cell adhesion was visualized using a Zeiss Axioscope 2 Plus fluorescent microscope.

Protein Adsorption Experiments

To assess the protein adsorption, we utilized the fluorescence microscopy technique. FITC-BSA was used for protein adsorption studies. The samples (coated/uncoated) were incubated with FITC-BSA (1 mg/mL, PBS, pH 7.4) at 37 °C. After 1 h, the samples were removed and washed with PBS for three times. The washed samples were then illuminated and imaged by a Zeiss Axioscope 2 Plus fluorescent microscope.

Percutaneous Infection Model in Mice

The animal experimental protocol was approved by the University of British Columbia Animal Care Committee. For the *in vivo* assessment of the coating activity against *P. mirabilis*, we utilized a mouse model of CAUTI previously developed and used by our groups.[9] Briefly, the catheters were coated using the similar procedure used for coating 10 Fr silicone urinary catheters. A 4 mm long piece of the catheter was cut from the tip of the catheter and re-assembled again. Under ultrasound guidance, the needle was advanced into the bladder and catheter piece pushed forward to fall into the bladder lumen. Following removal of the needle, the animals were recovered. One day after catheter implantation, the animals were anesthetized again, and *P. mirabilis* (5×10^5 CFU in 50 μL of PBS) was introduced percutaneously. After 3 days, the mice were sacrificed by CO_2 asphyxiation. Urine present in the bladder was collected and the number of bacteria quantified using spot plating and CFU determination. The indwelling catheters were removed and rinsed with sterile PBS and placed in Eppendorf tubes containing 1 mL of sterile PBS, and bacteria were dislodged and dispersed using a sonication water bath for 10 min. The supernatants were serially diluted and spotted on the agar plate to count the number of bacterial colonies attached to the surface of the catheter.

In Vitro Cytotoxicity Measurements

The samples (coatings on PU sheets: 5×5 mm^2) were fabricated as described earlier. To sterilize samples prior to testing, samples were immersed in 70% EtOH for 5 min, followed by extensive washing with PBS before adding them to 48-well plates. Afterward, RPMI media supplemented with 10% FBS and 1% P/S were added to each well (1 mL). The samples were incubated with the media for 12, 24, and 48 h. The supernatants were collected and kept at 4 °C until further use. T24 cells were cultured in 96-well plates at a seeding density of 1×10^5 cells/well for 24 h at 37 °C, 5% CO_2. Afterward, the medium was removed, and cells were washed with PBS prior to adding the collected media from the coatings. The cells were cultured with the collected media for 24 h prior to subjecting them to an MTS assay performed according to the manufacturer's protocol to measure

https://doi.org/10.1021/acsnanoscienceau.2c00040
ACS Nanosci. Au 2023, 3, 67−83

cell viability. Viability was assessed against control cells grown and cultured in fresh RPMI media. The experiment was done using media released from five independent samples in each coating group.

In Vivo Toxicity Analysis

We utilized a subcutaneous model in rats that was approved by the University of British Columbia Animal Care Committee to evaluate the *in vivo* biocompatibility of the DOPASIL coating. Briefly, an 8 mm incision was created on the backs of the animals just below the shoulders. The blunt dissection method was utilized to create pockets for the insertion of titanium implants (1×0.5 cm^2 titanium coils). After sample insertion, the incision was closed using sutures. The animals were recovered for 7 days at which point they were euthanized. The tissue which was in close contact with the implant was harvested and fixed in formalin. The fixed tissue was mounted in paraffin, sectioned, and stained using H&E. The images of stained samples were captured using an optical microscope (Zeiss Axioskop 2 plus, Carl Zeiss Microimaging Inc.) and analyzed by a board-certified pathologist.

Statistical Analysis

We reported standard deviation for both *in vitro* and *in vivo* data. The statistical analysis was carried out by a two-sample unpaired *t* test method by GraphPad.

■ ASSOCIATED CONTENT

Supporting Information

The Supporting Information is available free of charge at https://pubs.acs.org/doi/10.1021/acsnanoscienceau.2c00040.

DLS, SEM, TEM, and fluorescence microscopy data (PDF)

■ AUTHOR INFORMATION

Corresponding Authors

Dirk Lange − *Department of Urologic Sciences, University of British Columbia, Vancouver V6H 3Z6 British Columbia, Canada; The Stone Centre at Vancouver General Hospital, Vancouver V5Z 1M9 British Columbia, Canada*; Email: dirk.lange@ubc.ca

Jayachandran N. Kizhakkedathu − *Department of Chemistry, University of British Columbia, Vancouver V6T 1Z3 British Columbia, Canada; Centre for Blood Research, Life Science Institute and School of Biomedical Engineering, University of British Columbia, Vancouver V6T 1Z3 British Columbia, Canada; Department of Pathology and Laboratory Medicine, University of British Columbia, Vancouver V6T 1Z7 British Columbia, Canada*; orcid.org/0000-0001-7688-7574; Email: jay@pathology.ubc.ca

Authors

Hossein Yazdani-Ahmadabadi − *Department of Chemistry, University of British Columbia, Vancouver V6T 1Z3 British Columbia, Canada; Centre for Blood Research, Life Science Institute, University of British Columbia, Vancouver V6T 1Z3 British Columbia, Canada*

Kai Yu − *Centre for Blood Research, Life Science Institute, University of British Columbia, Vancouver V6T 1Z3 British Columbia, Canada; Department of Pathology and Laboratory Medicine, University of British Columbia, Vancouver V6T 1Z7 British Columbia, Canada*

Sara Khoddami − *Department of Urologic Sciences, University of British Columbia, Vancouver V6H 3Z6 British Columbia, Canada; The Stone Centre at Vancouver General Hospital, Vancouver V5Z 1M9 British Columbia, Canada*

Demian F. Felix − *Department of Urologic Sciences, University of British Columbia, Vancouver V6H 3Z6 British Columbia, Canada; The Stone Centre at Vancouver General Hospital, Vancouver V5Z 1M9 British Columbia, Canada*

Han H. Yeh − *Department of Mechanical Engineering, University of British Columbia, Vancouver V6T 1Z4 British Columbia, Canada*

Haiming D. Luo − *Department of Chemistry, University of British Columbia, Vancouver V6T 1Z3 British Columbia, Canada; Centre for Blood Research, Life Science Institute, University of British Columbia, Vancouver V6T 1Z3 British Columbia, Canada*

Igor Moskalev − *Vancouver Prostate Centre, University of British Columbia, Vancouver V6H 3Z6 British Columbia, Canada*

Qiong Wang − *Department of Materials Engineering, University of British Columbia, Vancouver V6T 1Z4 British Columbia, Canada*

Rizhi Wang − *Department of Materials Engineering, University of British Columbia, Vancouver V6T 1Z4 British Columbia, Canada; School of Biomedical Engineering, University of British Columbia, Vancouver V6T 1Z3 British Columbia, Canada*

Dana Grecov − *Department of Mechanical Engineering, University of British Columbia, Vancouver V6T 1Z4 British Columbia, Canada*

Ladan Fazli − *Vancouver Prostate Centre, University of British Columbia, Vancouver V6H 3Z6 British Columbia, Canada*

Complete contact information is available at: https://pubs.acs.org/10.1021/acsnanoscienceau.2c00040

Author Contributions

CRediT: **Hossein Yazdani-Ahmadabadi** conceptualization (equal), data curation (lead), formal analysis (equal), methodology (equal), writing-original draft (equal); **Kai Yu** data curation (supporting), formal analysis (supporting); **Sara Khoddami** data curation (supporting); **Demian F Felix** data curation (supporting), formal analysis (supporting); **Han H. Yeh** data curation (supporting), formal analysis (supporting); **Haiming Daniel Luo** data curation (supporting); **Igor Moskalev** data curation (supporting), methodology (supporting); **Qiong Wang** data curation (equal); **Rizhi Wang** formal analysis (equal), methodology (equal), supervision (equal); **Dana Grecov** formal analysis (equal), methodology (equal), supervision (equal); **Ladan Fazli** data curation (equal), formal analysis (equal), methodology (lead); **Dirk Lange** conceptualization (equal), funding acquisition (equal), investigation (equal), resources (equal), supervision (equal), writing-review & editing (equal); **Jayachandran N Kizhakkedathu** conceptualization (lead), formal analysis (lead), funding acquisition (lead), investigation (lead), project administration (lead), resources (lead), supervision (lead), writing-original draft (equal), writing-review & editing (lead).

Notes

The authors declare the following competing financial interest(s): The University of British Columbia has filed a patent application based on the research described with H.Y.A., K.Y., D.L., and J.N.K. as inventors.

■ ACKNOWLEDGMENTS

This work was funded by Canadian Institutes of Health Research (CIHR), Natural Sciences, Engineering Council of

Canada (NSERC), Canada Foundation for Innovation (CFI), and British Columbia Knowledge Development Fund. H.Y.-A. and H.D.L. would acknowledge NSERC NanoMat CREATE funding. H.D.L. acknowledges NSERC CGS-M and PGS-D scholarships. J.N.K. acknowledges Michael Smith Foundation for Health Research (MSFHR) for holding a Career Investigator Scholar award. J.N.K. is a Tier 1 Canada Research Chair. We also thank the Center for High-Throughput Phenogenomics (CHTP) at the University of British Columbia for providing us SEM and TEM images.

REFERENCES

(1) Li, M.; Neoh, K. G.; Kang, E. T.; Lau, T.; Chiong, E. Surface Modification of Silicone with Covalently Immobilized and Cross-linked Agarose for Potential Application in the Inhibition of Infection and Omental Wrapping. *Adv. Funct. Mater.* **2014**, *24*, 1631−1643.
(2) Zare, M.; Ghomi, E. R.; Venkatraman, P. D.; Ramakrishna, S. Silicone-Based Biomaterials for Biomedical Applications: Antimicrobial Strategies and 3D Printing Technologies. *J. Appl. Polym. Sci.* **2021**, *138*, 50969.
(3) Vogler, E. A. Protein Adsorption in Three Dimensions. *Biomaterials* **2012**, *33*, 1201−1237.
(4) Li, M.; Neoh, K. G.; Xu, L. Q.; Wang, R.; Kang, E. T.; Lau, T.; Olszyna, D. P.; Chiong, E. Erratum: Surface Modification of Silicone for Biomedical Applications Requiring Long-Term Antibacterial, Antifouling, and Hemocompatible Properties. *Langmuir* **2012**, *28*, 17859.
(5) Davies, D. Understanding Biofilm Resistance to Antibacterial Agents. *Nat. Rev. Drug Discovery* **2003**, *2*, 114−122.
(6) Busscher, H. J.; van der Mei, H. C.; Subbiahdoss, G.; Jutte, P. C.; van den Dungen, J. J. A. M.; Zaat, S. A. J.; Schultz, M. J.; Grainger, D. W. Biomaterial-Associated Infection: Locating the Finish Line in the Race for the Surface. *Sci. Transl. Med.* **2012**, *4*, 153rv10.
(7) Tran, C.; Yasir, M.; Dutta, D.; Eswaramoorthy, N.; Suchowerska, N.; Willcox, M.; McKenzie, D. R. Single Step Plasma Process for Covalent Binding of Antimicrobial Peptides on Catheters to Suppress Bacterial Adhesion. *ACS Appl. Bio Mater.* **2019**, *2*, 5739−5748.
(8) Lin, E. M. J.; Lay, C. L.; Subramanian, G. S.; Tan, W. S.; Leong, S. S. J.; Moh, L. C. H.; Lim, K. Control Release Coating for Urinary Catheters with Enhanced Released Profile for Sustained Antimicrobial Protection. *ACS Appl. Mater. Interfaces* **2021**, *13*, 59263−59274.
(9) Yu, K.; Lo, J. C. Y.; Yan, M.; Yang, X.; Brooks, D. E.; Hancock, R. E. W.; Lange, D.; Kizhakkedathu, J. N. Anti-Adhesive Antimicrobial Peptide Coating Prevents Catheter Associated Infection in a Mouse Urinary Infection Model. *Biomaterials* **2017**, *116*, 69−81.
(10) Yu, H.; Liu, L.; Li, X.; Zhou, R.; Yan, S.; Li, C.; Luan, S.; Yin, J.; Shi, H. Fabrication of Polylysine Based Antibacterial Coating for Catheters by Facile Electrostatic Interaction. *Chem. Eng. J.* **2019**, *360*, 1030−1041.
(11) Yu, H.; Liu, L.; Yang, H.; Zhou, R.; Che, C.; Li, X.; Li, C.; Luan, S.; Yin, J.; Shi, H. Water-Insoluble Polymeric Guanidine Derivative and Application in the Preparation of Antibacterial Coating of Catheter. *ACS Appl. Mater. Interfaces* **2018**, *10*, 39257−39267.
(12) Gao, Q.; Li, X.; Yu, W.; Jia, F.; Yao, T.; Jin, Q.; Ji, J. Fabrication of Mixed-Charge Polypeptide Coating for Enhanced Hemocompatibility and Anti-Infective Effect. *ACS Appl. Mater. Interfaces* **2020**, *12*, 2999−3010.
(13) Yong, Y.; Qiao, M.; Chiu, A.; Fuchs, S.; Liu, Q.; Pardo, Y.; Worobo, R.; Liu, Z.; Ma, M. Conformal Hydrogel Coatings on Catheters to Reduce Biofouling. *Langmuir* **2019**, *35*, 1927−1934.
(14) Guo, H.; Wen, C.; Tian, S.; Zhang, X.; Ma, Y.; Liu, X.; Yang, J.; Zhang, L. Universal Intraductal Surface Antifouling Coating Based on an Amphiphilic Copolymer. *ACS Appl. Mater. Interfaces* **2021**, *13*, 21051−21059.
(15) Smith, R. S.; Zhang, Z.; Bouchard, M.; Li, J.; Lapp, H. S.; Brotske, G. R.; Lucchino, D. L.; Weaver, D.; Roth, L. A.; Coury, A.; Biggerstaff, J.; Sukavaneshvar, S.; Langer, R.; Loose, C. Vascular Catheters with a Nonleaching Poly-Sulfobetaine Surface Modification Reduce Thrombus Formation and Microbial Attachment. *Sci. Transl. Med.* **2012**, *4*, 132.
(16) Yu, K.; Alzahrani, A.; Khoddami, S.; Cheng, J. T. J.; Mei, Y.; Gill, A.; Luo, H. D.; Haney, E. F.; Hilpert, K.; Hancock, R. E. W.; Lange, D.; Kizhakkedathu, J. N. Rapid Assembly of Infection-Resistant Coatings: Screening and Identification of Antimicrobial Peptides Works in Cooperation with an Antifouling Background. *ACS Appl. Mater. Interfaces* **2021**, *13*, 36784−36799.
(17) Yu, K.; Alzahrani, A.; Khoddami, S.; Ferreira, D.; Scotland, K. B.; Cheng, J. T. J.; Yazdani-Ahmadabadi, H.; Mei, Y.; Gill, A.; Takeuchi, L. E.; Yeung, E.; Grecov, D.; Hancock, R. E. W.; Chew, B. H.; Lange, D.; Kizhakkedathu, J. N. Self-Limiting Mussel Inspired Thin Antifouling Coating with Broad-Spectrum Resistance to Biofilm Formation to Prevent Catheter-Associated Infection in Mouse and Porcine Models. *Adv. Healthcare Mater.* **2021**, *10*, 2001573.
(18) Zhou, C.; Wu, Y.; Thappeta, K. R. V.; Subramanian, J. T. L.; Pranantyo, D.; Kang, E. T.; Duan, H.; Kline, K.; Chan-Park, M. B. Vivo Anti-Biofilm and Anti-Bacterial Non-Leachable Coating Thermally Polymerized on Cylindrical Catheter. *ACS Appl. Mater. Interfaces* **2017**, *9*, 36269−36280.
(19) Shalom, Y.; Perelshtein, I.; Perkas, N.; Gedanken, A.; Banin, E. Catheters Coated with Zn-Doped CuO Nanoparticles Delay the Onset of Catheter-Associated Urinary Tract Infections. *Nano Res.* **2017**, *10*, 520−533.
(20) Prateeksha, P.; Bajpai, R.; Rao, C. V.; Upreti, D. K.; Barik, S. K.; Singh, B. N. Chrysophanol-Functionalized Silver Nanoparticles for Anti-Adhesive and Anti-Biofouling Coatings to Prevent Urinary Catheter-Associated Infections. *ACS Appl. Nano Mater.* **2021**, *4*, 1512−1528.
(21) Ahmadabadi, H. Y.; Yu, K.; Kizhakkedathu, J. N. Surface Modification Approaches for Prevention of Implant Associated Infections. *Colloids Surf., B* **2020**, *193*, 111116.
(22) Geyer, F.; D'Acunzi, M. D.; Yang, C.; Müller, P.; Baumli, A.; Kaltbeitzel, V.; Mailänder, N.; Encinas, D.; Vollmer, H.; Butt, H.-J. How to Coat the Inside of Narrow and Long Tubes with a Super-Liquid-Repellent Layer—A Promising Candidate for Antibacterial Catheters. *Adv. Mater.* **2018**, *31*, 1801324.
(23) Zhang, S.; Wang, L.; Liang, X.; Vorstius, J.; Keatch, R.; Corner, G.; Nabi, G.; Davidson, F.; Gadd, Q.; Zhao, Q. Enhanced Antibacterial and Antiadhesive Activities of Silver-PTFE Nanocomposite Coating for Urinary Catheters. *ACS Biomater. Sci. Eng.* **2019**, *5*, 2804−2814.
(24) Zhang, S.; Liang, X.; Gadd, Q.; Zhao, Q. Superhydrophobic Coatings for Urinary Catheters To Delay Bacterial Bio Fi Lm Formation and Catheter-Associated Urinary Tract Infection. *ACS Appl. Bio Mater.* **2020**, *3*, 282−291.
(25) Sadrearhami, Z.; Shafiee, F. N.; Ho, K. K. K.; Kumar, N.; Krasowska, M.; Blencowe, A.; Wong, E. H. H.; Boyer, C. Antibiofilm Nitric Oxide-Releasing Polydopamine Coatings. *ACS Appl. Mater. Interfaces* **2019**, *11*, 7320−7329.
(26) Li, Y.; Liu, X.; Li, B.; Zheng, Y.; Han, Y.; Chen, D. F.; Yeung, K. W. K.; Cui, Z.; Liang, Y.; Li, Z.; Zhu, S.; Wang, X.; Wu, S. Near-Infrared Light Triggered Phototherapy and Immunotherapy for Elimination of Methicillin-Resistant Staphylococcus Aureus Biofilm Infection on Bone Implant. *ACS Nano* **2020**, *14*, 8157−8170.
(27) Mao, C.; Zhu, W.; Xiang, Y.; Zhu, Y.; Shen, J.; Liu, X.; Wu, S.; Cheung, K. M. C.; Yeung, K. W. K. Enhanced Near-Infrared Photocatalytic Eradication of MRSA Biofilms and Osseointegration Using Oxide Perovskite-Based P−N Heterojunction. *Adv. Sci.* **2021**, *8*, 2002211.
(28) Tan, L.; Li, J.; Liu, X.; Cui, Z.; Yang, X.; Zhu, S.; Li, Z.; Yuan, X.; Zheng, Y.; Yeung, K. W. K.; Pan, H.; Wang, X.; Wu, S. Rapid Biofilm Eradication on Bone Implants Using Red Phosphorus and Near-Infrared Light. *Adv. Mater.* **2018**, *30*, 1801808.
(29) Yazdani-Ahmadabadi, H.; Felix, D. F.; Yu, K.; Yeh, H. H.; Luo, H. D.; Khoddami, S.; Takeuchi, L. E.; Alzahrani, A.; Abbina, S.; Mei, Y.; Fazli, L.; Grecov, D.; Lange, D.; Kizhakkedathu, J. N. Durable Surfaces from Film-Forming Silver Assemblies for Long- Term Zero

Bacterial Adhesion without Toxicity. *ACS Cent. Sci.* **2022**, *8*, 546−561.
(30) Chernousova, S.; Epple, M. Silver as Antibacterial Agent: Ion, Nanoparticle, and Metal. *Angew. Chem., Int. Ed.* **2013**, *52*, 1636−1653.
(31) Richter, A. P.; Brown, J. S.; Bharti, B.; Wang, A.; Gangwal, S.; Houck, K.; Cohen Hubal, E. A.; Paunov, V. N.; Stoyanov, S. D.; Velev, O. D. An Environmentally Benign Antimicrobial Nanoparticle Based on a Silver-Infused Lignin Core. *Nat. Nanotechnol.* **2015**, *10*, 817−823.
(32) Cao, F.; Ju, E.; Zhang, Y.; Wang, Z.; Liu, C.; Li, W.; Huang, Y.; Dong, K.; Ren, J.; Qu, X. An Efficient and Benign Antimicrobial Depot Based on Silver-Infused MoS2. *ACS Nano* **2017**, *11*, 4651−4659.
(33) Lee, H.; Dellatore, S. M.; Miller, W. M.; Messersmith, P. B. Mussel-Inspired Surface Chemistry for Multifunctional Coatings. *Science* **2007**, *318*, 426−430.
(34) Feng, W.; Liu, N.; Gao, L.; Zhou, Q.; Yu, L.; Ye, X.; Huo, J.; Huang, X.; Li, P.; Huang, W. Rapid Inactivation of Multidrug-Resistant Bacteria and Enhancement of Osteoinduction via Titania Nanotubes Grafted with Polyguanidines. *J. Mater. Sci. Technol.* **2021**, *69*, 188−199.
(35) Xu, M.; Song, Q.; Gao, L.; Liu, H.; Feng, W.; Huo, J.; Jin, H.; Huang, L.; Chai, J.; Pei, Y.; Qu, X.; Li, P.; Huang, W. Single-Step Fabrication of Catechol-ε-Poly-L-Lysine Antimicrobial Paint That Prevents Superbug Infection and Promotes Osteoconductivity of Titanium Implants. *Chem. Eng. J.* **2020**, *396*, 125240.
(36) Lv, Y.; Yang, H. C.; Liang, H. Q.; Wan, L. S.; Xu, Z. K. Nanofiltration Membranes via Co-Deposition of Polydopamine/Polyethylenimine Followed by Cross-Linking. *J. Membr. Sci.* **2015**, *476*, 50−58.
(37) Chen, T.; Liu, T.; Su, T.; Liang, J. Self-Polymerization of Dopamine in Acidic Environments without Oxygen. *Langmuir* **2017**, *33*, 5863−5871.
(38) Salomäki, L.; Marttila, H.; Kivelä, T.; Ouvinen, J. E.; Lukkari, J. Ff Ects of PH and Oxidants on the First Steps of Polydopamine Formation: A Thermodynamic Approach. *J. Phys. Chem. B* **2018**, *122*, 6314−6327.
(39) Ponzio, M.; Barthès, V.; Bour, J.; Michel, M.; Bertani, P.; Hemmerlé, J.; d'Ischia, M.; Ball, V. Oxidant Control of Polydopamine Surface Chemistry in Acids: A Mechanism-Based Entry to Superhydrophilic-Superoleophobic Coatings. *Chem. Mater.* **2016**, *28*, 4697−4705.
(40) Zhang, C.; Ou, Y.; Lei, W.; Wan, L.; Ji, J.; Xu, Z. CuSO4/H2O2-Induced Rapid Deposition of Polydopamine Coatings with High Uniformity and Enhanced Stability. *Angew. Chem., Int.* **2016**, *55*, 3054−3057.
(41) Zdziennicka, A.; Krawczyk, J.; Jańczuk, B. Wettability and Adhesion Work Prediction in the Polymer-Aqueous Solution of Surface Active Agent Systems. *Colloids Interfaces* **2018**, *2*, 21.
(42) Jiang, X.; Wang, Y.; Li, M. Selecting water-alcohol mixed solvent for synthesis of polydopamine nano-spheres using solubility parameter. *Sci. Rep.* **2014**, *4*, 6070.
(43) Ai, K.; Liu, Y.; Ruan, C.; Lu, L.; Lu, G. M. Sp2 C-Dominant N-Doped Carbon Sub-Micrometer Spheres with a Tunable Size : A Versatile Platform for Highly Effi Cient Oxygen-Reduction Catalysts. *Adv. Mater.* **2013**, *25*, 998−1003.
(44) Park, H.; Park, S.; Lee, H. K.; Hong, J. H. Material-Selective Polydopamine Coating in Dimethyl Sulfoxide. *ACS Appl. Mater. Interfaces* **2020**, *12*, 49146−49154.
(45) Sato, T.; Hamada, Y.; Sumikawa, M.; Araki, S.; Yamamoto, H. Solubility of Oxygen in Organic Solvents and Calculation of the Hansen Solubility Parameters of Oxygen. *Ind. Eng. Chem. Res.* **2014**, *53*, 19331−19337.
(46) You, I.; Jeon, H.; Lee, K.; Do, M.; Seo, Y. C.; Lee, H. A.; Lee, H. Polydopamine Coating in Organic Solvent for Material-Independent Immobilization of Water-Insoluble Molecules and Avoidance of Substrate Hydrolysis. *J. Ind. Eng. Chem.* **2017**, *46*, 379−385.
(47) https://www.caymanchem.com/pdfs/21992.pdf (accessed Feb 9, 2022).
(48) Mei, Y.; Yu, K.; Lo, J. C. Y.; Takeuchi, L. E.; Hadjesfandiari, N.; Yazdani-Ahmadabadi, H.; Brooks, D. E.; Lange, D.; Kizhakkedathu, J. N. Polymer-Nanoparticle Interaction as a Design Principle in the Development of a Durable Ultrathin Universal Binary Antibiofilm Coating with Long-Term Activity. *ACS Nano* **2018**, *12*, 11881−11891.
(49) Gurunathan, S.; Qasim, M.; Park, C.; Yoo, H.; Choi, D. Y.; Song, H.; Park, C.; Kim, J. H.; Hong, K. Cytotoxicity and Transcriptomic Analysis of Silver Nanoparticles in Mouse Embryonic Fibroblast Cells. *Int. J. Mol. Sci.* **2018**, *19*, 3618.
(50) Gliga, A. R.; Skoglund, S.; Odnevall Wallinder, I.; Fadeel, B.; Karlsson, H. L. Size-Dependent Cytotoxicity of Silver Nanoparticles in Human Lung Cells: The Role of Cellular Uptake, Agglomeration and Ag Release. *Part. Fibre Toxicol.* **2014**, *11*, 11.
(51) Sundaram, H. S.; Han, X.; Nowinski, A. K.; Brault, N. D.; Li, Y.; Ella-Menye, J. R.; Amoaka, K. A.; Cook, K. E.; Marek, P.; Senecal, K.; Jiang, S. Achieving One-Step Surface Coating of Highly Hydrophilic Poly(Carboxybetaine Methacrylate) Polymers on Hydrophobic and Hydrophilic Surfaces. *Adv. Mater. Interfaces* **2014**, *1*, 1400071.
(52) Elwood, C. N.; Lo, J.; Chou, E.; Crowe, A.; Arsovska, O.; Adomat, H.; Miyaoka, R.; Tomlinson-Guns, E.; Monga, M.; Chew, B. H.; Lange, D. Understanding Urinary Conditioning Film Components on Ureteral Stents: Profiling Protein Components and Evaluating Their Role in Bacterial Colonization. *Biofouling* **2013**, *29*, 1115−1122.
(53) Scotland, K. B.; Kung, S. H. Y.; Chew, B. H.; Lange, D. Uropathogens Preferentially Interact with Conditioning Film Components on the Surface of Indwelling Ureteral Stents Rather than Stent Material. *Pathogens* **2020**, *9*, 764.
(54) Rozilah, A.; Jaafar, C. N.; Sapuan, S. M.; Zainol, I.; Ilyas, R. A. The Effects of Silver Nanoparticles Compositions on the Mechanical, Physiochemical, Antibacterial, and Morphology Properties of Sugar Palm Starch Biocomposites for Antibacterial Coating. *Polymers* **2020**, *12*, 2605.
(55) Pakseresht, S.; Alogaili, A. W. M.; Akbulut, H.; Placha, D.; Pazdziora, E.; Klushina, D.; Konvičková, Z.; Kratošová, G.; Holešová, S.; Martynková, G. S. Silver/Chitosan Antimicrobial Nanocomposites Coating for Medical Devices: Comparison of Nanofiller Effect Prepared via Chemical Reduction and Biosynthesis. *J. Nanosci. Nanotechnol.* **2019**, *19*, 2938−2942.
(56) Wilks, S. A.; Fader, M. J.; Keevil, C. W. Novel Insights into the Proteus Mirabilis Crystalline Biofilm Using Real-Time Imaging. *PLoS One* **2015**, *10*, No. e0141711.
(57) Stapleton, F.; Stretton, S.; Papas, E.; Skotnitsky, C.; Sweeney, D. F. Silicone Hydrogel Contact Lenses and the Ocular Surface. *Ocul. Surf.* **2006**, *4*, 24−43.
(58) Brooks, T.; Keevil, C. W. A Simple Artificial Urine for the Growth of Urinary Pathogens. *Lett. Appl. Microbiol.* **1997**, *24*, 203−206.

https://doi.org/10.1021/acsnanoscienceau.2c00040
ACS Nanosci. Au 2023, 3, 67−83